PlanetiQ Radio Occultation: Preliminary Comparative Analysis of Neutral Profiles vs. COSMIC and NWP Models

Ibrahim F. Ahmed * , Mohammed Alheyf , Mohamed S. Yamany

Posted Date: 17 April 2024

doi: 10.20944/preprints202404.1137.v1

Keywords: GNSS Radio Occultation; PlanetiQ; COSMIC; GFS; ECMWF

 doi:10.20944/preprints202404.1137.v1

Article

PlanetiQ Radio Occultation: Preliminary Comparative Analysis of Neutral Profiles vs. COSMIC and NWP Models

Ibrahim F. Ahmed [1,*], Mohammed Alheyf [2] and Mohamed S. Yamany [3,4]

[1] Assistant Professor, Construction Eng. & Utilities Department, Faculty of Engineering, Zagazig University, Zagazig 44159, Egypt. Ibrahim_fouad_ghonim@yahoo.com; ifahmd@eng.zu.edu.eg
[2] Assistant Professor, Department of Civil Engineering, College of Engineering, King Saud University, P.O. Box 800, Riyadh 11421, Saudi Arabia. alheyf@ksu.edu.sa
[3] Assistant Professor, Department of Construction Engineering, Faculty of Engineering, Zagazig University, Zagazig 44159, Egypt. msyamany@eng.zu.edu.eg; mohamedyamany9@gmail.com
[4] Post-doctoral Research Associate, Department of Civil and Architectural Engineering and Construction Management, University of Wyoming, 1000 E. University Ave., Dept. 3295, Laramie, WY 82071, Unite States. myamany@uwyo.edu.
* Correspondence: Ibrahim_fouad_ghonim@yahoo.com or ifahmd@eng.zu.edu.eg

Featured Application: Our study's findings have practical implications for weather forecasting, climate research, and atmospheric modeling. By evaluating the distribution of Radio Occultation (RO) observations from the PlanetiQ mission and comparing them with existing datasets, we contribute to enhancing atmospheric profiling accuracy. This has significant benefits for weather forecasts, climate projections, and environmental monitoring, especially considering that PlanetiQ's RO profiles have not been assessed until now.

Abstract: Radio Occultation (RO) is pivotal for profiling the neutral and ionized atmosphere, with the PlanetiQ mission, via its GNOMES satellites, striving to establish an advanced atmospheric observing system. However, an assessment of the spatiotemporal distributions of PlanetiQ observations and comparisons with reliable datasets are lacking. This study addresses this gap by examining the temporal and spatial distribution of RO observations from PlanetiQ during its initial 198 operational days in 2023, alongside comparisons with COSMIC and Numerical Weather Prediction (NWP) models. Data from GN02, GN03, and GN04 satellites, yielding 1099, 1313, and 1843 RO events per day respectively, were analyzed. The satellite constellation's observations demonstrate a generally well-distributed pattern, albeit minor deficiencies in equatorial and polar regions. Single-profile comparisons with COSMIC data reveal strong correlations for pressure, temperature, Water Vapor Pressure (WVP), and refractivity profiles, with temperature exhibiting larger variations (RMSE = 1.24°C). Statistical analyses confirm statistically insignificant differences between PlanetiQ and COSMIC profiles at the same spatio-temporal coordinates. Comparisons with NWP models show slight differences with GFS, with overall RMSE values of 0.23 mb (WVP), 0.6 mb (pressure), 1.3 (refractivity), and 1.5°C (temperature). However, assessments against GFS/ECMWF models indicate overall compatibility, with insignificant differences between PlanetiQ profiles and models observations.

Keywords: GNSS radio occultation; PlanetiQ; COSMIC; GFS; ECMWF

1. Introduction

Presently, the RO method is recognized as one of the most accurate, expeditious, and straightforward approaches for acquiring atmospheric profiles [1]. In pursuit of advancing satellite weather observations, PlanetiQ, established in 2012, has dedicated its efforts to the development, launch, and operation of the initial commercial constellation of GNSS-RO weather satellites. Known as GNOMES (GNSS Navigation and Occultation Measurement Satellites), this groundbreaking

 doi:10.20944/preprints202404.1137.v1

constellation comprises 20 Low Earth Orbiting (LEO) satellites, each equipped with the cutting-edge fourth-generation "Pyxis" RO sensor. This technological advancement positions PlanetiQ at the forefront of satellite-based weather observation, promising heightened precision and efficiency in global atmospheric monitoring. For further details, refer to PlanetiQ's official technology page [2]. The GNOMES constellation, set to collect over 50,000 soundings per day, approximately 400 million data observations, is poised to revolutionize weather forecasting, space weather prediction, and climate analytics [2].

The exploration RO profiles stand as a central tenet in the realm of atmospheric science research, with a pronounced focus on harnessing the capabilities of numerical weather prediction (NWP) models and the Constellation Observing System for Meteorology, Ionosphere, and Climate (COSMIC) satellite. Myriad investigations have delved into the meticulous comparison of RO profiles sourced from diverse missions with those derived from the esteemed COSMIC satellite or intricate NWP models. The overarching objective of these inquiries lies in the discerning scrutiny of the precision and dependability of RO measurements in capturing nuanced atmospheric parameters [3].

This study aims to analyze the spatiotemporal distribution of PlanetiQ observations during its initial 198 operating days, filling a crucial gap in prior research. By examining how RO observations are distributed across Earth vectors, annual days, and daily hours, the research seeks to understand the strengths and limitations of the preliminary observations conducted by the PlanetiQ mission. To assess the reliability of the obtained atmospheric profiles, comparisons will be made with COSMIC RO profiles and NWP models. Through this comparative analysis, the study aims to provide insights into the overall quality of the PlanetiQ mission's data and its potential integration with established atmospheric models, thereby contributing to advancements in atmospheric science and forecasting capabilities.

2. Literature Review

[4] conducted a comprehensive exploration of Earth's atmosphere through the lens of RO measurements emanating from the Global Positioning System (GPS). This pioneering research laid a foundational cornerstone for subsequent studies that leveraged advanced NWP models to meticulously validate and refine RO profiles. The seamless integration of cutting-edge NWP models facilitates a holistic evaluation of the congruence between observed RO profiles and those prognosticated by sophisticated numerical simulations.

Comparative analysis plays a crucial role in understanding the impact of observing systems, offering nuanced insights into the effectiveness of GNSS-RO data across temporal epochs [5]. A recent scholarly exploration has delved into the comparative analysis of Binhu and COSMIC-2 RO data, highlighting the avant-garde exploration of Earth's atmosphere facilitated by innovative GNSS-RO technology [6]. This research sheds light on the unique contributions and capabilities of these observational systems.

Furthermore, studies have elucidated differences between GPS RO and radiosonde atmosphere profiles, providing valuable insights into atmospheric variabilities. Particularly, research in regions like Egypt, led by [7], contributes to our understanding of the atmospheric dynamics in specific geographical contexts. These comparative analyses collectively contribute to advancing our comprehension of atmospheric phenomena and optimizing the utilization of GNSS-RO data in various scientific applications.

Radio Occultation Concept

The RO method with an onboard space receiver has been comprehensively elucidated by several researchers, including [4,8], and [9]. In essence, this technique involves the precise measurement of how radio waves emitted by a GPS satellite experience bending due to refractive index gradients before reaching a LEO satellite [10]. The geometric arrangement is illustrated in Figure 1, with the LEO typically positioned approximately 700 km above Earth's surface, while the GPS satellite orbits at around 22,000 km above the surface [11].

 doi:10.20944/preprints202404.1137.v1

Upon intersecting the atmosphere, the trajectory of the radio wave undergoes a bending phenomenon at the tangent point, expressed as the bending angle (α) e.g. [12]. This angle is subsequently translated into measurements encompassing pressure, temperature, Water Vapor Pressure (WVP), and refractivity within the neutral atmosphere. In ionized mediums, this bending angle contributes to determining Total Electronic Content (TEC) e.g. [13]. Originally developed during the early stages of interplanetary exploration, the RO technique has significantly advanced our comprehension of planetary atmospheres within the solar system, as underscored by e.g. [14].

The methodology involves deploying a RADAR transmitter on a spacecraft positioned beyond the target planet's atmosphere, coupled with a receiver stationed on Earth's surface. As the spacecraft becomes occulted by the planet's limb, electromagnetic rays traverse various atmospheric layers, undergoing bending and deceleration. This intricate process allows the receiver to glean valuable insights into the vertical structure of the planet's ionosphere and neutral atmosphere, as demonstrated by e.g. [15].

The adaptation of the RO technique to study Earth's atmosphere became feasible with the introduction of the U.S. Global Positioning System (GPS) in the early 1980 e.g. [16]. With the addition of the Russian GLONASS system, the emerging European GALILEO system, and the Chinese BEIDOU system, a diverse array of transmitter platforms became available for probing Earth's atmosphere. In the contemporary context, even a limited number of spaceborne GNSS receivers on LEO could establish a global observation system with unparalleled spatial and temporal resolution e.g. [17].

By receiving signals from all four major GNSS constellations—GPS, GLONASS, Galileo, and Beidou—Pyxis stands out as the only GPS-RO sensor in its compact size capable of providing over ten times the data of existing sensors and routinely probing into the lowest atmospheric layers where severe weather events unfold. Figure 1 provides a schematic representation of the RO geometry for one RO event for the LEO satellites PlanetiQ. Where r_G, r_L are the vectors of GNSS and PlanetiQ satellite positions, V_G, V_L are the vectors of GNSS and PlanetiQ satellites velocities, θ_L the angle between the line connecting the Earth's center and the PlanetiQ and the ray direction, θ_G the angle between the line connecting the Earth's center and the GNSS satellite and the ray direction, a the impact parameter, α the signal bending angle e.g. [18].

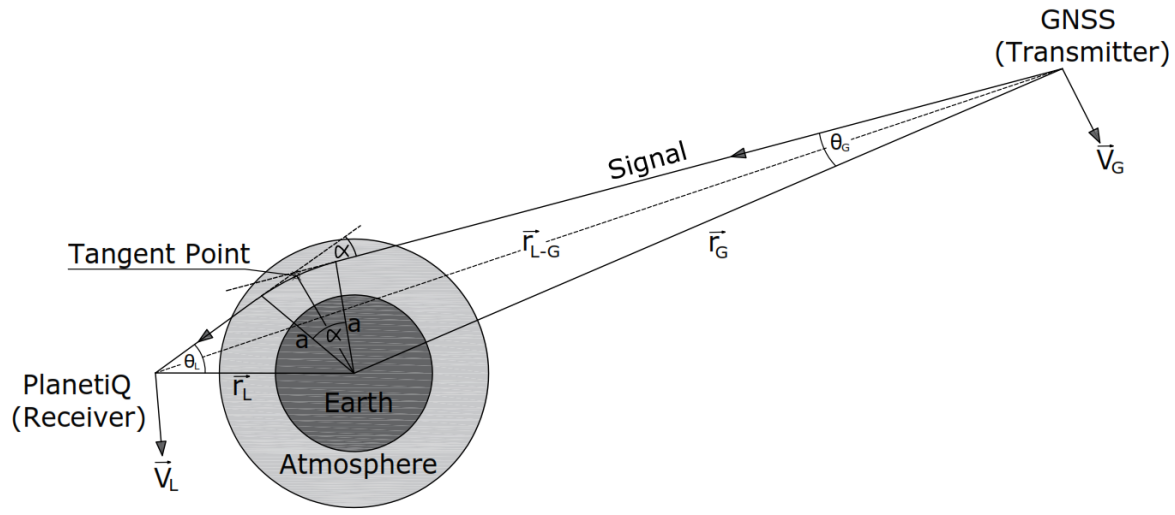

Figure 1. Occultation event geometry, defining important location and angular variables of an RO event. Adapted from [19].

In the context of the neutral atmosphere, the refractivity (N), a dimensionless parameter represented as $N=10^6(n - 1)$, where 'n' denotes the refractive index, can be formally expressed in relation to atmospheric conditions. Refractivity is intricately linked to atmospheric pressure (P)

 doi:10.20944/preprints202404.1137.v1

measured in hectopascals, temperature (T) in kelvins, and water vapor partial pressure (Pw) in hectopascals [20].

$$N = 77.6\frac{P}{T} + 3.73 \times 10^5 \frac{P_w}{T^2} \quad (1)$$

In the framework of a locally spherically symmetric atmosphere, a ray adheres to Bouguer's law, implying that the impact parameter in equation (2) remains constant for a specific ray within the geometric optics approximation [21].

$$a = rn(r)sin(\theta_L) \quad (2)$$

The total refractive bending angle α, as a function of rt (i.e., the radius of the ray at the tangent point), is given by [14]. in equation (3), which can be further simplified to equation (4) given that a(r) is a monotonic function and using the substitution x=n(r)r [20]:

$$\alpha(a) = -2a\int_{r_t}^{\infty} \frac{1}{n}\frac{dn}{dr}\frac{dr}{\sqrt{(nr)^2 - a^2}} \quad (3)$$

$$\alpha(a) = -2a\int_{r_t}^{\infty} \frac{1}{n}\frac{dn}{dx}\frac{dx}{\sqrt{x^2 - a^2}} \quad (4)$$

In the existence of a ducting layer, the impact parameter 'a' exhibits a non-monotonic behavior concerning the radial distance 'r' within and immediately below the ducting layer, as demonstrated by [22]. Additionally, the calculation of 'a' requires an alternative method, specifically not adhering to equation (4). To address this, a more suitable approach, described in detail by [22], is employed for solving equation (3) in the presence of the ducting layer. Once the bending angle profile is provided, the refractive index function 'n(r)' is determined by inverting equation (5) using the Abel inversion technique, as outlined by [14]. From refractivity, pressure, temperature, and WVP, refractivity can be calculated.

$$n(r) = exp\left[\frac{1}{\pi}\int_a^{\infty} \frac{\alpha(x)dx}{\sqrt{x^2 - a^2}}\right] \quad (5)$$

3. Research Methodology

The wetPrf profiles from the PlanetiQ mission encompass atmospheric occultation profiles with detailed moisture information, incorporating parameters such as atmospheric pressure, geometric height, temperature, WVP, and retrieved refractivity. Similar to the COSMIC comparison, the observed refractivity profiles are recorded in the wetPrf data obtained from the PlanetiQ mission. The research methodology is visually depicted in Figure 2.

COSMIC has been a pioneering force in advancing our understanding of the Earth's atmosphere. Deployed in the mid-2000s, COSMIC consists of a constellation of microsatellites equipped with RO sensors. These sensors utilize signals from GNSS to probe the Earth's atmosphere, providing precise measurements of atmospheric parameters. Over the years, COSMIC has contributed invaluable data for various atmospheric studies, serving as a benchmark for comparing and validating RO data, such as that obtained from the PlanetiQ mission [23].

 doi:10.20944/preprints202404.1137.v1

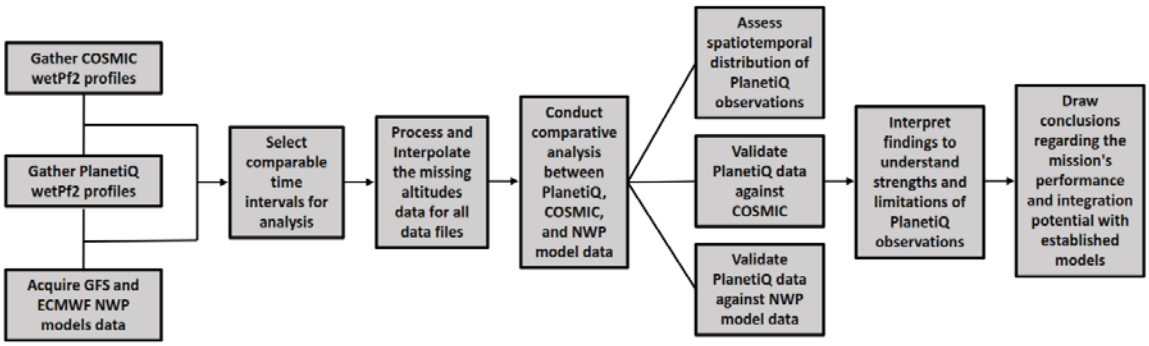

Figure 2. Research methodology flow chart.

The Global Forecast System (GFS), developed by the National Centers for Environmental Prediction (NCEP), is a widely utilized NWP model. Renowned for its global coverage and operational forecasting capabilities, the GFS model assimilates observational data to generate forecasts for various atmospheric variables. As a key player in meteorological modeling, the GFS serves as a significant reference point for assessing the accuracy of RO data, providing a basis for comparison with the PlanetiQ mission profiles [25].

The European Centre for Medium-Range Weather Forecasts (ECMWF) operates a state-of-the-art NWP model, recognized for its high-resolution simulations and global forecasting prowess. ECMWF assimilates a diverse range of observational data to produce accurate and timely weather forecasts. In the context of comparing with the PlanetiQ RO data, ECMWF's NWP model offers a robust benchmark, reflecting advancements in atmospheric modeling techniques. The comprehensive and globally influential nature of ECMWF's predictions positions it as a key player in assessing the accuracy and reliability of RO data from the PlanetiQ mission [24].

The ongoing study involves a comprehensive analysis of PlanetiQ pressure, temperature, WVP, and refractivity profiles for the online available profiles in 2023 year. This evaluation relies on dependable mission profiles from COSMIC and GFS and ECMWF NWP models. The aim is to assess and compare the accuracy and reliability of PlanetiQ's atmospheric data against these well-established sources, providing valuable insights into the mission's performance in capturing essential atmospheric parameters.

The “wetPf2” profiles from the PlanetiQ RO mission were gathered and processed for the comparison, offering a vertical resolution of 100 m within the altitude range of 0-60 km. The “wetPf2” data format mirrors that of “wetPrf” profiles generated by COSMIC. “wetPf2” constitutes an atmospheric occultation profile inclusive of moisture information. Utilizing gridded analysis or short-term forecasting, the separation of pressure, temperature, and moisture contributions to refractivity is achieved. This file undergoes interpolation to 100-meter height levels. These profiles provided a substantial dataset, averaging more than 1700 profiles globally per day during the study period. For the comparison process, the background data used in the 1DVAR analysis were sourced from the GFS and ECMWF analysis, similar to the COSMIC comparison.

Atmospheric data comprising PlanetiQ's pressure, temperature, WVP, and refractivity profiles is accessible on the COSMIC-UCAR website (https://cdaac-www.cosmic-.ucar.edu/). These datasets are formatted in wetPrf NetCDF files and encompass the time intervals from Day Of Year (DOY) 2023.095 to DOY 2023.125 and DOY 2023.199 to DOY 2023.365, representing the initial 198 data days of the year 2023. The study period incorporates information from three LEO satellites: GN02, GN03, and GN04. Figure 3 illustrates the availability of RO Events (ROE) in the UCAR-COSMIC datasets throughout the study period.

During the first 31 days, exclusive data from GN02 (2023.095 to DOY 2023.125) contributes to an average of approximately 700 ROE per day. Subsequently, the period from 2023.199 to 2023.243 sees combined data from GN02 and GN03, resulting in an average of around 2450 ROE per day. From

 doi:10.20944/preprints202404.1137.v1

DOY 2023.244 to DOY 2023.338, GN02 provides atmospheric data independently. Finally, GN02 and GN03 satellites collectively provide profiles for the remaining days of the year 2023.

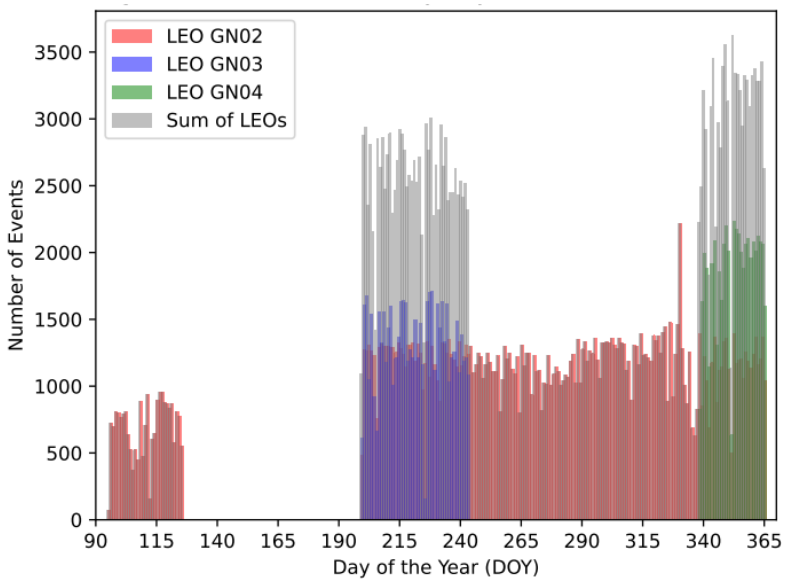

Figure 3. PlanetiQ ROE number through study period DOYs based on LEO satellites.

The COSMIC-UCAR datasets offer GFS and ECMWF profiles for comparing with PlanetiQ wetPrf files, aligned with observational data. The "avnPrf" represents the GFS NWP model file format, presenting atmospheric data in the NetCDF format akin to the "wetPf2" file. The temperature, pressure, and moisture profiles are derived from NCEP AVN 12-hour forecast files, co-located with occultation profiles. These profiles serve as the initial estimate for determining moisture below 10km in the real-time CDAAC process and facilitate comparison. Additionally, the "echPrf" stands as the ECMWF NWP model file format, providing atmosphere data in the same NetCDF format as the "wetPf2" and "avnPrf" files.

An intricate analysis is conducted utilizing Python and bash scripts on Ubuntu. All PlanetiQ wetPf2 files are acquired from the COSMIC-UCAR website during the days of 2023. To juxtapose PlanetiQ profiles with COSMIC constellations profiles, a meticulous comparison methodology is employed. This involves a singular profile comparison using two observations from distinct missions (one checkpoint) situated at the same location and time. Additionally, multiple observations from various missions, located within the same coordinates and temporal parameters (checkpoints), are considered, with a difference of 1° in latitude and longitude and 1 hour in time. Each "checkpoint" entails discerning the disparities between two observations from PlanetiQ and COSMIC, with a thorough analysis of spatial and temporal differences. To obtain checkpoints with minimal disparities, ten days of global COSMIC data are downloaded.

To conduct a comprehensive assessment and comparison between the PlanetiQ observations and the GFS and ECMWF NWP models, a systematic approach is adopted. Over 300 randomly selected daily checkpoints are employed for each of the 198 study days. This meticulous selection process enables the thorough examination and evaluation of disparities between individual PlanetiQ observations and their counterparts in the GFS and ECMWF NWP models. The outcome is a detailed profile of differences across all checkpoints throughout the study period.

The disparities between PlanetiQ profiles and the corresponding profiles from COSMIC and NWP models are quantified and presented through various metrics, including mean diff. values, Root Mean Square Error (RMSE), and mean diff.%. The mean diff.% is calculated as (Diff.% = (O - B) / O), where 'O' represents the PlanetiQ observation and 'B' denotes the observation from the comparative COSMIC or NWP models. These differences are not only depicted in profiles but also spatially visualized on maps, showcasing the distribution of variations concerning altitude, latitude, and longitude.

 doi:10.20944/preprints202404.1137.v1

To ascertain the statistical significance of the differences between the observations of the PlanetiQ mission and the COSMIC and NWP models profiles, f-test and independent t-tests assuming equal variances are conducted across various checkpoint profiles. F-test is used to check the difference significance of the variances and t-test to check the difference significance between the profiles observations. This rigorous statistical analysis provides a robust understanding of the significance and reliability of the observed disparities.

4. Results and Discussion

The research findings will be delineated across three principal sections. The initial section will elucidate the dispersion of PlanetiQ's ROE across both spatial and temporal dimensions. Subsequently, the second section will delineate the disparities between PlanetiQ observations and those derived from COSMIC, with a meticulous examination of their statistical significance via appropriate tests. Finally, the third section will scrutinize the disparities vis-à-vis the NWP models, specifically GFS and ECMWF, while rigorously evaluating the statistical significance of these variances.

4.1. PlanetiQ Observations Spatial and Temporal Distribution

Figure 4 depicts the worldwide distribution of ROE for the three satellites within the PlanetiQ constellation throughout the entire study duration. GN02, GN03, and GN04 have operational periods lasting 198, 55, and 28 days, respectively, with average daily occurrences of 1099, 1313, and 1843 ROE. The global coverage is consistently uniform, excluding the Polar Regions and a specific area delineated by 30° to 50° longitude and 40° to 60° latitude.

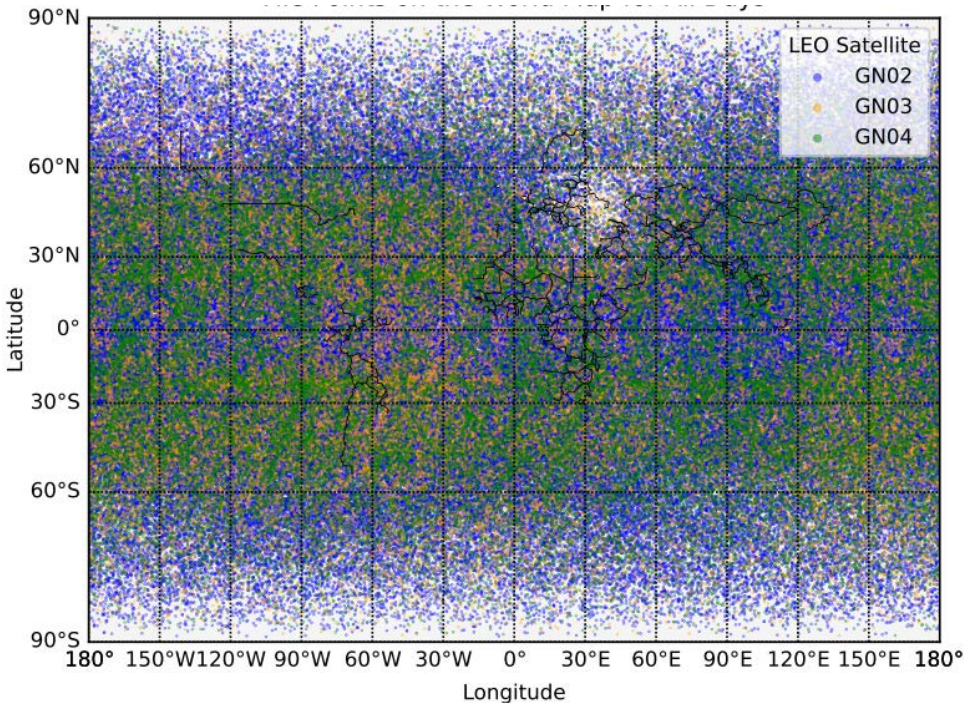

Figure 4. Global distribution of PlanetiQ ROE through the study period based on LEO satellites.

Figure 5 illustrates the geographic distribution of each LEO satellite, considering both latitude and longitude tracking. It is noteworthy that the operational duration of GN02 exceeds that of GN03 and GN04 by approximately 3.5 and 7 times, respectively, throughout the entire study period. All LEO satellites exhibit extensive observational coverage within the latitude range of 10° to 30° and -20° to -50°, with moderate and limited distribution coverage observed at the Equator and the poles, respectively. The distribution along the longitude is predominantly uniform, except for a specific region around 30° longitude, where there is a notable deficit in observation coverage. Interestingly,

 doi:10.20944/preprints202404.1137.v1

there is a slight increase in observation numbers in western longitudes compared to eastern longitudes within this deficient region.

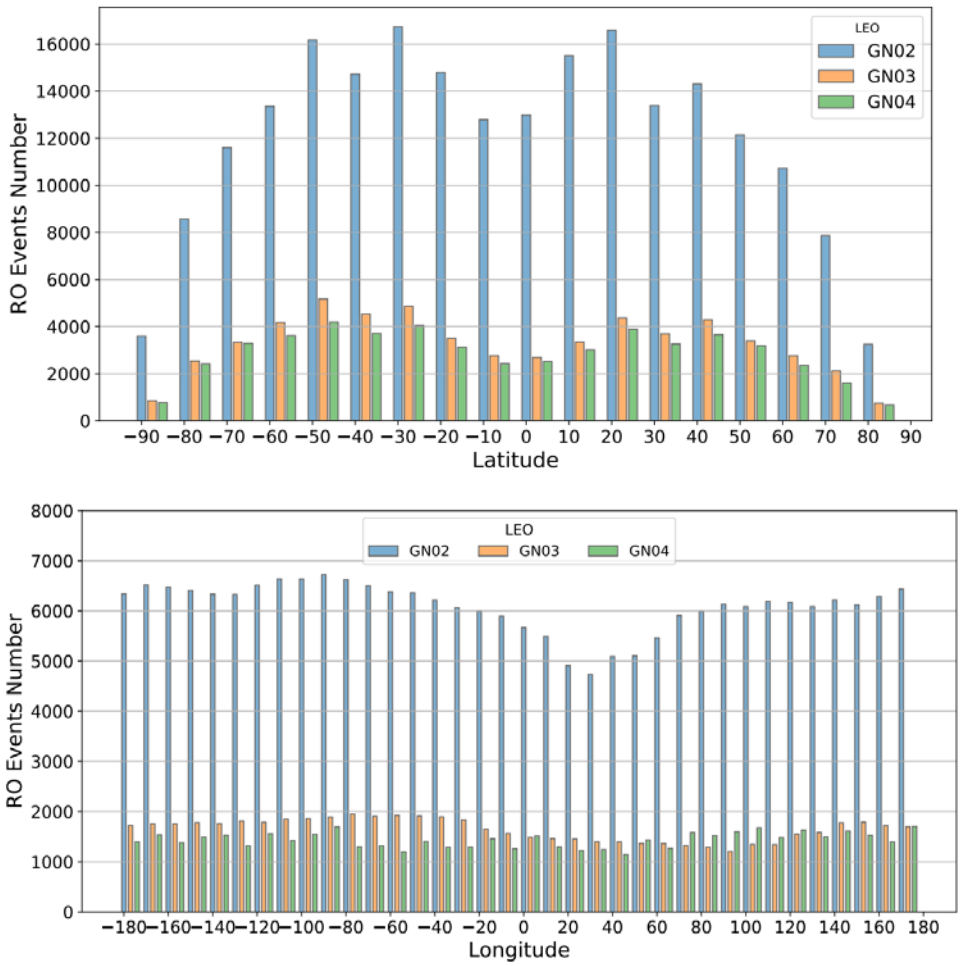

Figure 5. Distribution of study period PlanetiQ ROE through the longitude and latitude based on LEO satellites.

The distribution of observations throughout the day, as depicted in Figure 6, reveals that the twelfth hour boasts the highest total number of observations compared to other hours, while the twenty-third hour exhibits the lowest. Specifically for GN02, the eighth hour registers the maximum total number of observations, contrasting with the minimum observed in the twenty-third hour. In the case of LEO GN03, the thirteenth hour records the maximum number of observations, whereas the third hour records the minimum. Similarly, for LEO GN04, the twelfth hour sees the highest number of observations, and the nineteenth hour reflects the minimum. The overall occurrence of observations is nearly uniform across the day hours, except for variations in hours 0, 3, 22, and 23.

Preprints.org (www.preprints.org) | NOT PEER-REVIEWED | Posted: 17 April 2024 doi:10.20944/preprints202404.1137.v1

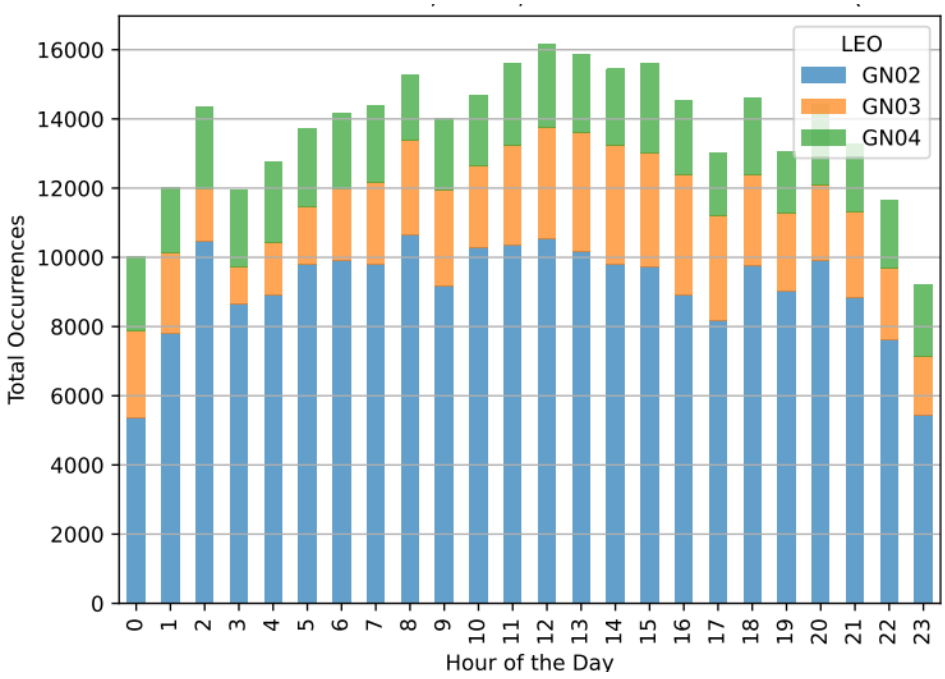

Figure 6. Total occurrence of PlanetiQ ROE with day hours through the study period. .

Figure 7 depicts the daily occurrence of observations for each GNSS satellite. Each GNSS constellation is represented by distinct color bars, and the distribution is based on the average number of observations solely during their operational days. Overall, the average occurrence of observations for all GNSS satellites is relatively uniform, with the maximum diff. in occurrence numbers not exceeding 5 observations. Notably, G01 and E01 in GPS and Galileo, respectively, exhibit comparatively lower average daily observation numbers.

To specify, the average daily number of observations for GPS, Galileo, GLONASS, and Beidou satellites amounts to 440, 413, 392, and 489 ROE/day, respectively. The notable increase in the number provided by the Beidou constellation can be attributed to its synchronization of operating days with those of both GN02 and GN04.

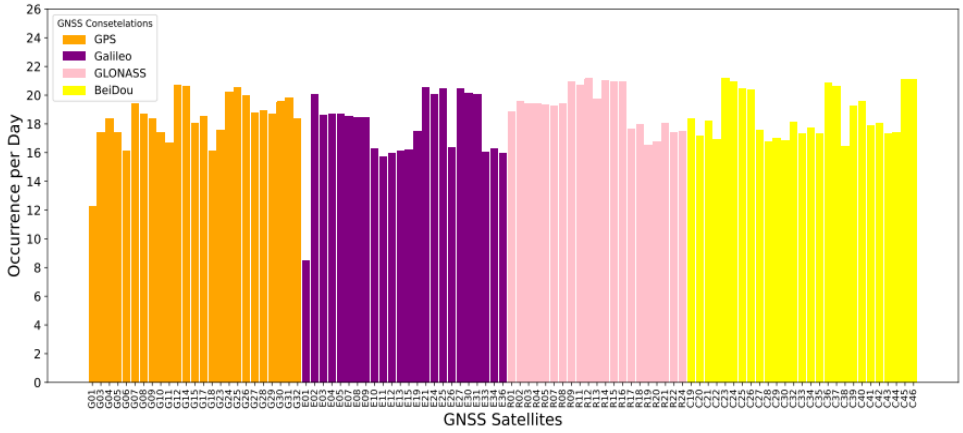

Figure 7. Average occurrence number for each of GNSS constellations satellites.

Figure 8 shows the total occurrence of RO events along the latitude and the longitude referencing to the observation GNSS transmitter constellation. The observed distribution of ROE across various 20° longitude intervals provides a nuanced perspective on the geographic prevalence of signals emanating from GNSS constellations, namely GPS, Beidou, Galileo, and GLONASS. The distinctive patterns within each constellation's data showcase specific regions where these signals are more prevalent or less pronounced. For instance, the GPS constellation exhibits a substantial peak of 5556

 doi:10.20944/preprints202404.1137.v1

events in the longitude interval of -80 to -100, while experiencing a minimum of 3618 events in the 20 to 40 longitude range. Similarly, Beidou constellation demonstrates notable variations, reaching a maximum of 4968 events in the -80 to -100 longitude interval and a minimum of 3843 events in the 40 to 60 longitude range. Galileo constellation peaks at 5039 events between -60 to -80 in longitude and exhibits a minimum of 3672 events in the 20 to 40 longitude interval. GLONASS constellation, mirrors this trend with maximum and minimum occurrences of 4843 and 3812 events, respectively, in the -80 to -100 and 20 to 40 longitude intervals.

The overall total occurrences across all constellations sum up to 87624, with an average occurrence of 4868 events per longitude interval. This cumulative average provides a consolidated metric, reflecting the combined influence of all GNSS constellations across the analyzed longitudes. The results emphasize the significance of considering multiple constellations in understanding the distribution of RO events, as each contributes uniquely to the observed patterns. Such insights can prove invaluable for refining satellite-based positioning systems and enhancing our comprehension of atmospheric phenomena across diverse geographical regions.

The distribution of RO events from the PlanetIQ mission, analyzed across 10° latitude intervals for GNSS constellations, reveals distinct patterns and variations in signal occurrences. For the GPS constellation, the data illustrates a pronounced concentration with the maximum occurrences of 8985 events in the 0 to 10° latitude interval, highlighting a notable prevalence in lower latitudes. Conversely, the minimum occurrences of 1227 events in the 80 to 90° latitude interval indicate a reduced presence in Polar Regions. Similar trends are observed for the Beidou and Galileo constellations, with their respective maximum occurrences of 7513 and 8026 events in the 0 to 10° latitude interval, and minimum occurrences of 1304 and 1105 events in the 80 to 90° latitude interval. Notably, the GLONASS constellation exhibits a robust distribution, peaking at 11612 events in the 0 to 10° latitude interval. The minimum occurrences of 1013 events in the 80 to 90° latitude interval indicate a consistent presence even in higher latitudes. The cumulative average occurrence, calculated as the sum of individual constellation averages, amounts to 5154.41 events per interval. These findings underscore the diverse spatial characteristics of GNSS signals and their varying strengths across latitudinal zones. Such insights contribute to a comprehensive understanding of atmospheric phenomena and aid in refining satellite-based positioning systems for enhanced accuracy and reliability.

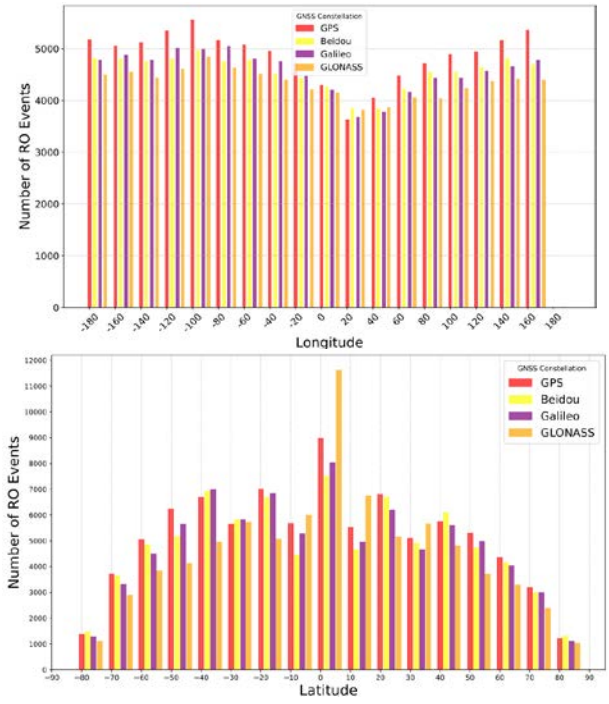

Figure 8. Distribution of study period PlanetiQ RO events through the longitude and latitude based on GNSS satellites.

 doi:10.20944/preprints202404.1137.v1

The geographic distribution of observations from PlanetIQ LEO Satellites GN02 and GN04 on DOY 342 is visualized in Figure 9. The figure provides a comprehensive overview of observations from various GNSS constellations, including GPS, GLONASS, Galileo, and BeiDou. The total number of observations for GN02 and GN04 on DOY 3023-342 are 689 ROE and 1143 ROE, respectively. Notably, the observations from the GPS constellation account for 455 ROE, GLONASS for 440 ROE, Galileo for 444 ROE, and BeiDou for 493 ROE.

The analysis further explores hourly observations, revealing distinctive patterns throughout the day. The maximum observations occur at 20:00 hr, totaling 131, while the minimum observations are recorded at 08:00 hr, amounting to 31. This temporal analysis provides valuable insights into the dynamic nature of observations during the specified day.

Additionally, the spatial distribution analysis unveils intriguing details. The maximum 1° latitude with 21 observations is found at -25.0°, while the minimum is observed at -90.0° with a single observation. In terms of longitude, the maximum longitude is 131° with 14 observations, contrasting with the minimum at 130° with only one observation.

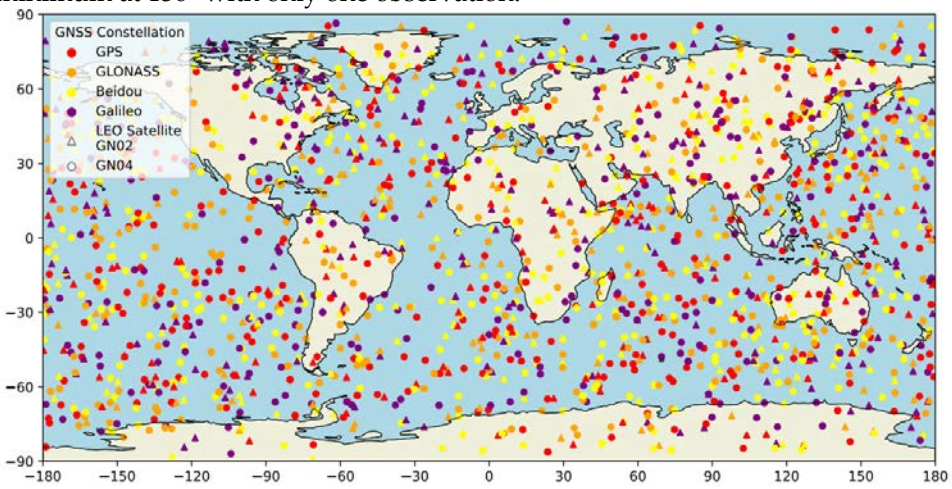

Figure 9. Global distribution of PlanetiQ RO events for DOY 342 based on GNSS constellations and LEO satellites. .

4.2. PlanetiQ-COSMIC Profiles Comparison

4.2.1. Single Profile Comparison

A comparative analysis of atmospheric profiles retrieved from the PlanetiQ and COSMIC missions was conducted, focusing on key meteorological parameters such as pressure, temperature, WVP, and refractivity (Figure 10). Our investigation encompassed altitudes ranging from the surface up to 20 kilometers. The mean differences between the two datasets revealed subtle distinctions in atmospheric conditions. Specifically, the PlanetiQ dataset's mean pressure increased by 0.26 mb when compared to the COSMIC dataset. The temperature exhibited a marginal decrease of -0.02°C in PlanetiQ profiles, indicating a subtle cooling trend relative to the COSMIC profiles. The WVP content displayed a small reduction of -0.08 mb in the PlanetiQ dataset, signifying a nuanced divergence in humidity profiles. Refractivity differences revealed a decrease of -0.23 in PlanetiQ compared to COSMIC, implying variations in the atmospheric refractive index.

Examining specific altitudes, our analysis at 10 kilometers revealed negligible differences in pressure (0.00 mb) and a more pronounced cooling trend in Temperature (-0.16°C) for PlanetiQ versus COSMIC. The WVP content showed a marginal increase of 0.01 mb in PlanetiQ, suggesting subtle humidity fluctuations. Refractivity differences at 10 kilometers exhibited a positive shift of 0.15 in PlanetiQ, pointing to differences in atmospheric composition. At 20 kilometers, the findings demonstrated a rise in pressure (0.13 mb) in PlanetiQ, coupled with a more significant warming trend in Temperature (0.40°C). The WVP content showed minimal differences (0.00 mb), while the refractivity exhibited a slight increase of 0.01 in PlanetiQ.

Preprints.org (www.preprints.org) | NOT PEER-REVIEWED | Posted: 17 April 2024 doi:10.20944/preprints202404.1137.v1

These findings contribute valuable insights into the comparative analysis of atmospheric profiles from PlanetiQ and COSMIC missions, highlighting nuanced changes in meteorological factors at different altitudes. The observed variations underscore the importance of considering mission-specific characteristics in atmospheric research and contribute to the ongoing refinement of global atmospheric models.

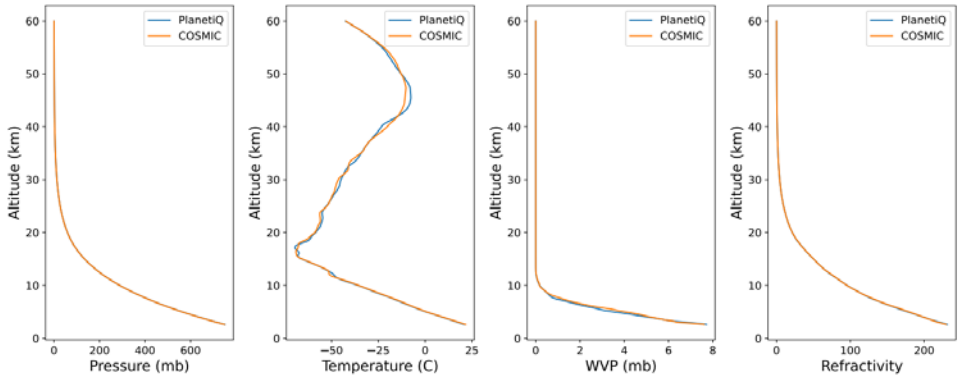

Figure 10. Pressure, temperature, WVP and refractivity profiles for PlanetiQ-COSMIC collocated observation.

The analysis of atmospheric profiles from both PlanetIQ and COSMIC datasets reveals minor differences across several key parameters (Figure 11). In the pressure comparison, a mean difference of 0.15 mb with a root mean square (RMS) of 0.31 mb was observed. Noteworthy fluctuations were observed, with a minimum difference of -0.12 mb and a maximum difference of 1.39 mb at different altitudes. Similarly, temperature varies, with a mean difference of 0.17°C and an RMS of 1.24°C. The temperature differences range from a minimum of -1.14°C to a maximum of 3.15°C. For WVP, the mean diff. is -0.04 mb, with an RMS of 0.12 mb. The fluctuations range from a minimum of -0.60 mb to a maximum of 0.35 mb. Finally, in the case of Refractivity, a mean diff. of -0.10 is observed, with an RMS of 0.57. The differences in Refractivity span from a minimum of -2.53 to a maximum of 2.45. These findings underscore the variations between the PlanetIQ and COSMIC atmospheric profiles, emphasizing the importance of understanding these distinctions for accurate meteorological assessments.

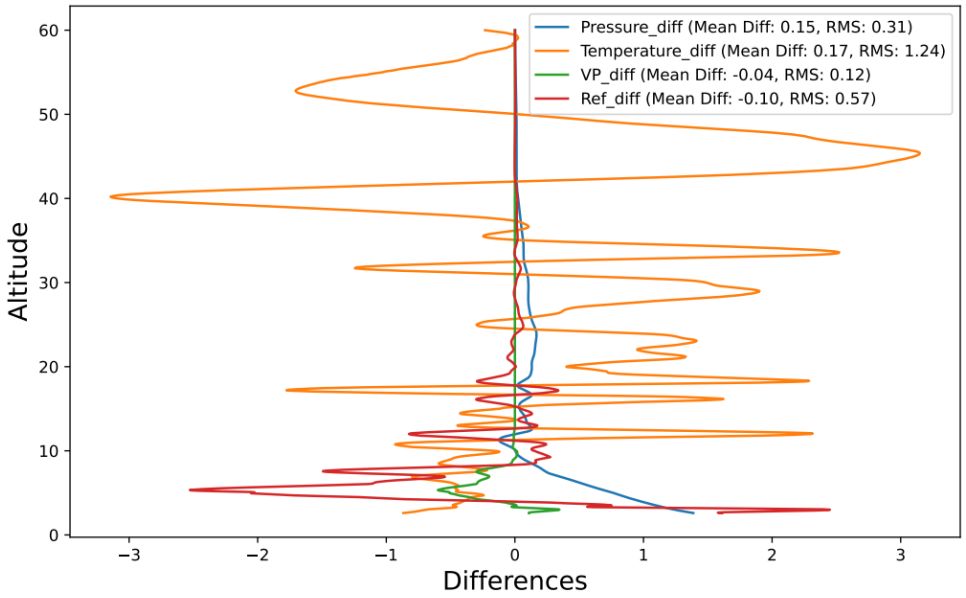

Figure 11. Differences values between pressure, temperature, WVP and refractivity profiles.

Figure 12 shows the regression between PlanetiQ and COSMIC profiles over the same time and location. The examination of pressure profiles from both the PlanetiQ and COSMIC datasets reveals

 doi:10.20944/preprints202404.1137.v1

an exceptional correlation (r = 1.00), indicating a perfect linear relationship. The mean difference of 0.15 mb, RMSE of 0.31 mb, and mean absolute value (MAV) of 0.16 mb suggest a generally close agreement between the two datasets. These results signify the reliability of pressure measurements at different altitudes. Notably, the altitudes corresponding to the minimum and maximum differences provide valuable insights, with the minimum occurring at 10.1 km (0.00 mb) and the maximum at 2.6 km (1.39 mb), which may indicate specific atmospheric phenomena at these levels.

The temperature profiles show a strong correlation (r = 1.00) between the PlanetiQ and COSMIC datasets. The mean difference of 0.17°C, RMSE of 1.24°C, and MAV of 0.95°C indicate a consistent agreement, albeit with larger variations compared to pressure. These results highlight the overall accuracy of Temperature measurements, with the altitudes associated with the minimum and maximum differences at 31.0 km (0.00°C) and 45.4 km (3.15°C), respectively. Larger differences at higher altitudes may be indicative of sensitivity to specific atmospheric conditions.

The WVP profiles demonstrate a perfect correlation (r = 1.00) between the PlanetiQ and COSMIC datasets. The mean difference of -0.04 mb, RMSE of 0.12 mb, and MAV of 0.04 mb imply a near overall agreement. These findings support the reliability of WVP measurements at different altitudes. The altitude variations, with the least difference at 30.3 km (0.00 mb) and the largest at 5.3 km (0.60 mb), emphasize the significance of altitude-dependent variances and may provide insights into atmospheric moisture distribution.

Analyzing Refractivity profiles reveals a strong correlation (r = 1.00) between the PlanetiQ and COSMIC datasets. The mean difference of -0.10, RMSE of 0.57, and MAV of 0.25 indicate a strong agreement with some variability. These results suggest the overall accuracy of refractivity measurements, with the altitudes associated with the minimum and maximum discrepancies at 46.1 km (0.00) and 5.35 km (2.53), respectively. Variations at different altitudes may be indicative of distinct atmospheric scattering properties.

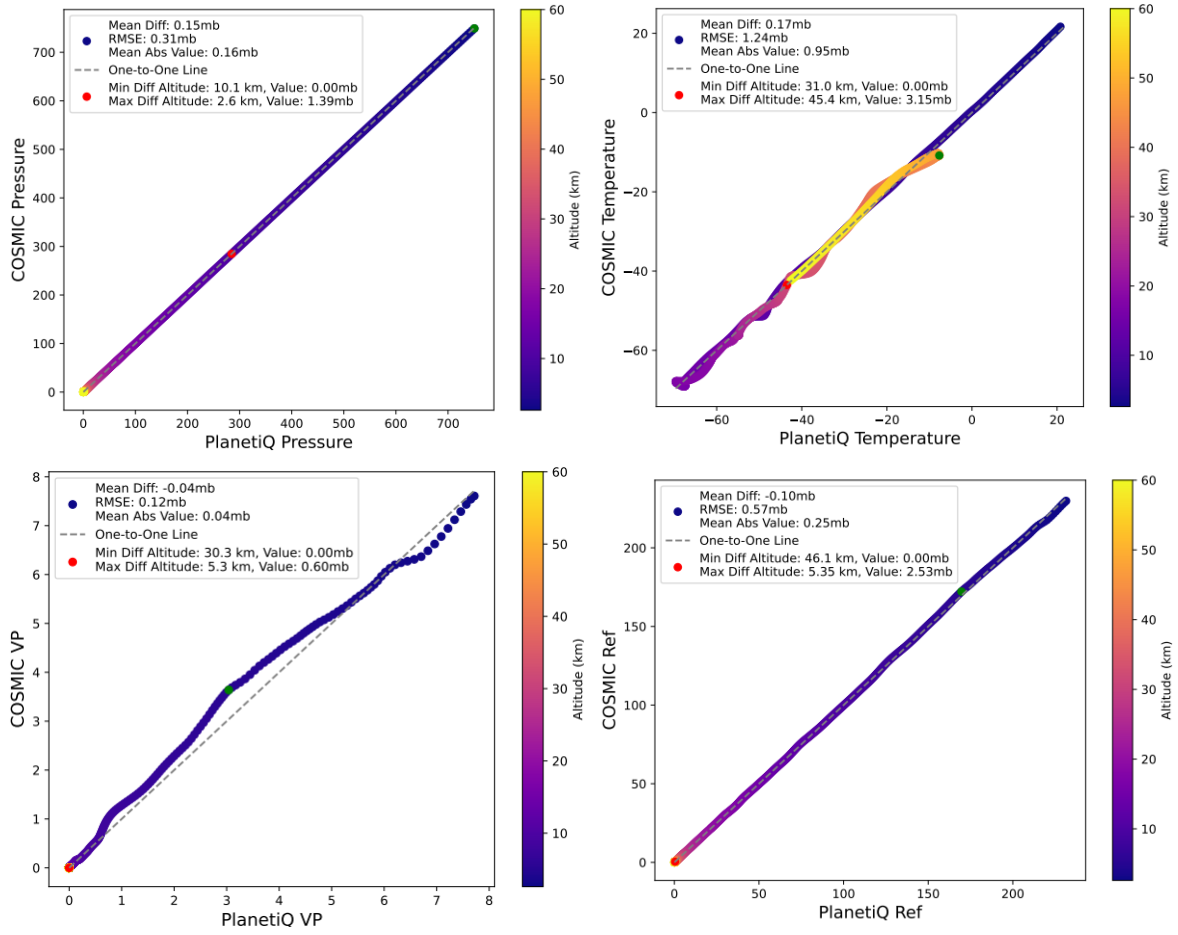

 doi:10.20944/preprints202404.1137.v1

Figure 12. Regression between PlanetiQ and COSMIC profiles observations for all variables indicating the mean diff., RMSE and mean absolute diff. values.

Upon subjecting the PlanetIQ and COSMIC atmospheric profiles to t-tests for individual variables, it becomes apparent that there exist no statistically significant distinctions at the designated location and time. The t-test outcomes for each variable further support the conclusions drawn from the preceding f-tests.

In the instance of pressure, the f-test indicates a lack of significant difference in variances between the two profiles, with an F-Stat of 0.00 and a p-value of 0.988. Consequently, the t-test for pressure was conducted under the assumption of equal variances, yielding a T-Stat of 0.015 alongside a p-value of 0.988. This result, surpassing the Tcritical value of 1.962 at confidence level of 95%, solidifies the inference that the marginal pressure differentials observed between the two profiles lack statistical significance.

Similarly, in the domain of WVP, the f-test shows no significant variance difference, with an F-Stat of 0.212 and a p-value of 0.645. Consequently, the t-test for WVP was performed under the assumption of equal variances, manifesting a T-Stat of -0.461 and a p-value of 0.645. According to the Tcritical value of 1.962 at 95%, the non-significant p-value reinforces the absence of meaningful disparities in WVP between the PlanetIQ and Cosmic profiles.

The t-test examination for Temperature, under the premise of equal variances based on the f-test results (F-Stat = 0.020, p-value = 0.887), yields a T-Stat of 0.142 and a p-value of 0.887. This outcome, consistent with a Tcritical value of 1.962, signifies that the minute temperature fluctuations between the two profiles are statistical insignificant.

Finally, the f-test implies no significant variance difference (F-Stat = 0.001, p-value = 0.974). Consequently, the t-test produces a T-Stat of -0.032 and a p-value of 0.974. With the Tcritical value at 1.962, the non-significant p-value reaffirms the absence of noteworthy distinctions in the reference values between the PlanetIQ and Cosmic profiles.

In summary, the consistent lack of statistical significance in the t-test outcomes for each variable, coupled with the non-significant variance differences indicated by the f-tests, substantiates the overarching conclusion that there are no statistical significant differences between the PlanetIQ and COSMIC profiles at the designated location and time.

4.2.2. Multi-Profile Comparison

The spatial and temporal differences between the PlanetiQ and COSMIC observations are used to classify data into three groups (G1, G2, and G3). G1 consists of 9 check points that represent difference in observations time and location of 15 minutes and 0.25° in latitude and longitude, respectively. G2 is made up of 15 check points that signify difference in observations time and location of 30 minutes and 0.5° in latitude and longitude, respectively. G3 consists of 18 check points representing difference in observations time and location of 60 minutes and 1° in latitude and longitude, respectively.

Figure 13 depicts a comprehensive view of the RMSE distributions across 12 distinct groups, each reflecting varying temporal and spatial differences between PlanetIQ and COSMIC profiles. The groups (G1, G2, G3) are characterized by differences in time intervals (15, 30, and 60 minutes) and spatial resolutions (0.25°, 0.5°, and 1° in latitude and longitude), with of 9, 15, 18 check points, respectively. G1, which has minimal spatiotemporal changes between observations, seems to have less medians and ranges across all variables than G2 and G3. Notably, each boxplot captures the spread of RMSE values across these categories. Key descriptive statistics, such as median, quartiles, and whisker ranges, provide insight into the central tendency and variability of the RMSE. For instance, regarding the pressure in G1, the median RMSE is 0.29 mb with an interquartile range (IQR) of 0.07 mb, suggesting relatively low variability. In contrast, the pressure in G2 exhibits a wider IQR (0.21 mb) and five outliers, indicating higher variability and potential discrepancies in profiles with greater temporal and spatial differences. The absence of outliers in the pressure of G3 suggests robust agreement within the specified temporal and spatial bounds. Similar findings were observed in the

 doi:10.20944/preprints202404.1137.v1

refractivity, temperature, and WVP groups. These findings underscore the sensitivity of RMSE to temporal and spatial disparities, offering valuable insights into the reliability of altitude-pressure profiles under different observational conditions. The absence of outliers in certain groups indicates acceptable agreement, but the existence of outliers prompts consideration of data refinement for more accurate atmospheric profiling. Overall, the detailed analysis of RMSE distributions in Figure 13 provides a nuanced understanding of the reliability of PlanetIQ and COSMIC profiles under varying observational conditions, which will drive future data assimilation strategies and model improvements.

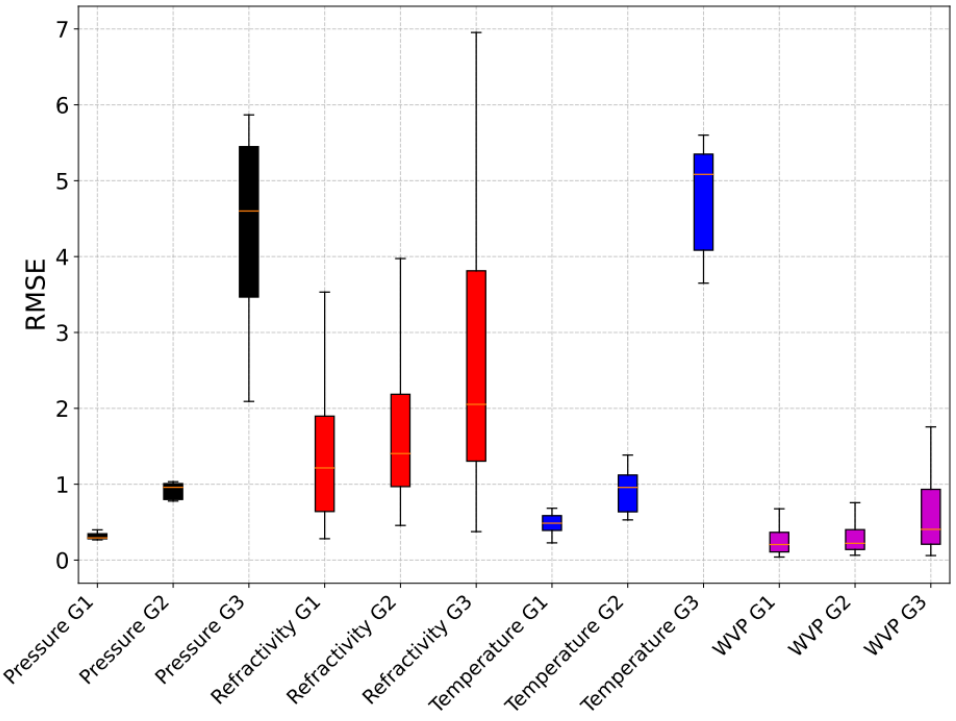

Figure 13. Boxplot for RMSE values for groups 1, 2 and 3 for each variable.

The results depicted in Figure 14 provide a comprehensive overview of the mean difference, RMSE, and mean difference percentage profiles for all atmospheric variables. These profiles compare the G1 check points profiles from the PlanetiQ and COSMIC. The maximum difference in pressure is approximately 0.2 mb, with a mean of 0.06 mb and a maximum RMSE of 0.4 mb. The altitude associated with the largest mean difference is 6.6 km, while the maximum RMSE occurs at 10.2 km. The mean difference percentage at the height of greatest RMSE is 0.04%.

Regarding refractivity, the profiles exhibit a maximum difference of 1.71, a mean difference of 0.002%, and a maximum RMSE of 4.7. The altitude corresponding to the largest mean difference is 3.0 km, where the maximum RMSE appears at 3.5 km. The mean difference percentage at the altitude of maximum RMSE is 0.19%.

Temperature profiles reveal a maximum difference of 1.52°C, a mean difference of -0.06 °C, and a maximum RMSE of 3.25°C. The height associated with the largest mean difference is 27.1 km, while the maximum RMSE occurs at 38.6 km. The mean difference percentage at the altitude of maximum RMSE is 0.47%.

For WVP, the profiles indicate a maximum difference of 0.3232 mb, a mean difference of -0.005 mb, and a maximum RMSE of 0.9 mb. The altitude corresponding to the maximum mean difference is 3.0 km, while the maximum RMSE occurs at 3.5 km. The mean difference percentage at the altitude of maximum RMSE is 1.65%. Notably, the difference percentage for WVP appears to be relatively larger than that for the other variables, reflecting the sensitivity of the observation values in relation to the differences.

 doi:10.20944/preprints202404.1137.v1

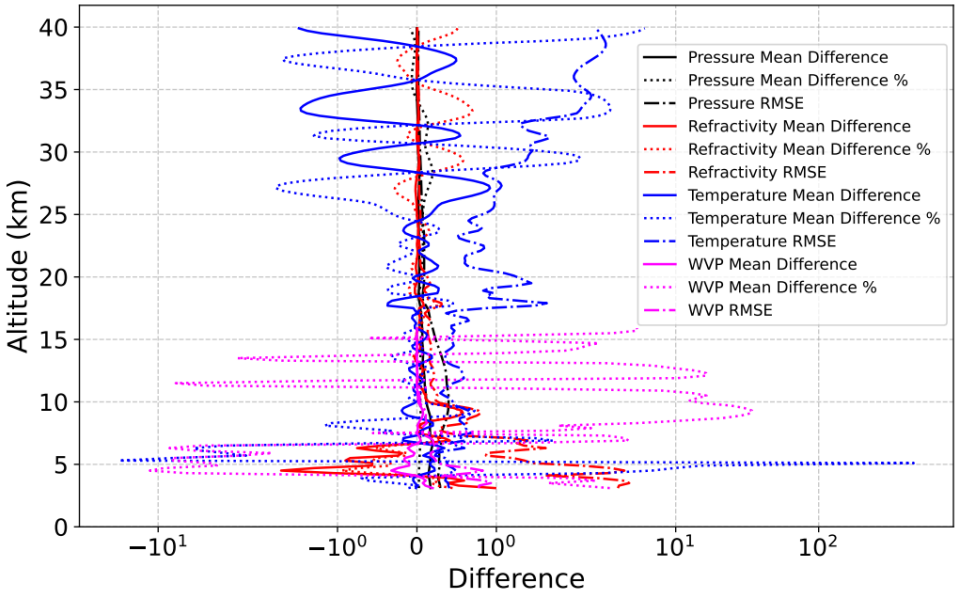

Figure 14. Mean diff., mean diff.% and RMSE between PlanetiQ and COSMIC profiles for G1 for all variables.

Figure 15 presents a detailed comparison of G2 data from PlanetiQ and COSMIC for the key atmospheric variables: pressure, refractivity, temperature, and WVP. Pressure profiles indicate a maximum difference of 2.55 mb, a mean difference of -0.07 mb, and a maximum RMSE of 9.3 mb, with notable variations at 11.9 and 3.6 km altitudes. The refractivity profiles reveal a maximum difference of 0.72, a mean difference of -0.01, and a maximum RMSE of 6.2, with significant disparities at 3.3 and 3.6 km altitudes. Temperature profiles display a maximum difference of 1.06°C, a mean difference of 0.02°C, and a maximum RMSE of 3.5°C, with distinct variations at 40.0 km altitude. The WVP profiles indicate a maximum difference of 0.2 mb, a mean difference of 0.01 mb, and a maximum RMSE of 0.96 mb, with notable differences at 3.3 and 3.6 km altitudes. Overall, these findings underscore significant disparities in the atmospheric variables between PlanetiQ and COSMIC datasets, which emphasizes variations in mean difference, RMSE, and percentage of mean difference across different altitudes.

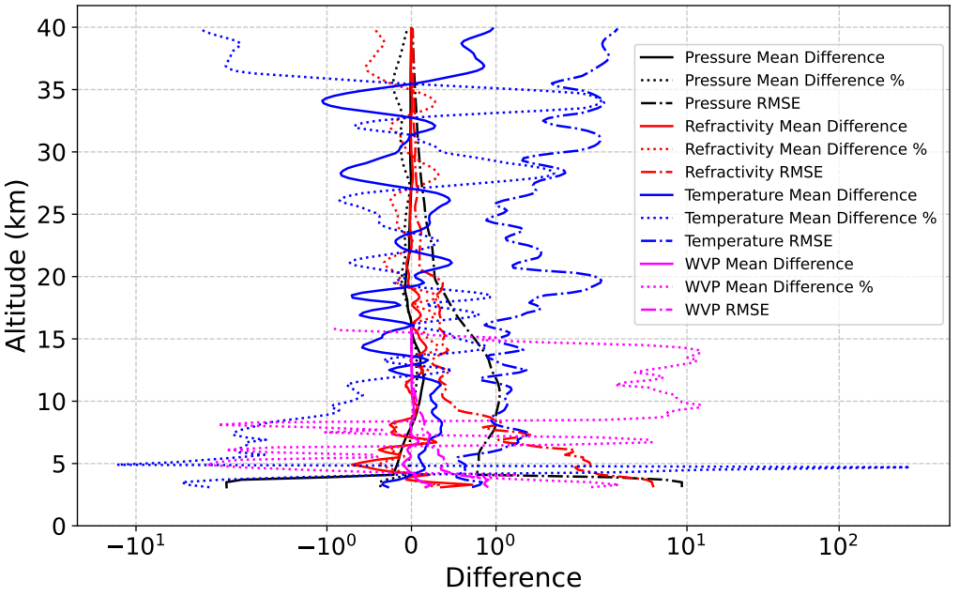

Figure 15. Mean diff., mean diff.% and RMSE between PlanetiQ and COSMIC profiles for G2 for all variables.

 doi:10.20944/preprints202404.1137.v1

Figure 16 provides an extensive overview of mean differences, RMSE, and percentage of mean differences for significant atmospheric variables pressure, refractivity, temperature, and WVP within G3 data. For pressure, the profiles indicate a maximum difference of 1 mb, a mean difference of -0.29 mb, and a maximum RMSE of 6 mb, with significant variations at altitudes of 34.5 and 10.9 km. The refractivity profiles show a maximum difference of 1.76, a mean difference of -0.12 (unitless), and a maximum RMSE of 10.7, emphasizing disparities at 3.1 km and 3.0 km elevations. The temperature profiles display a maximum difference of 1.66 °C, a mean difference of 0.1 °C, and a maximum RMSE of 7.9 °C, with significant differences at 33.6 km and 17.8 km altitudes. WVP profiles reveal a maximum difference of 0.28 mb, a mean difference of -0.04 mb, and a maximum RMSE of 2.75 mb, highlighting variations at 3.1 and 3.0 km altitudes. These outcomes underscore substantial differences between the PlanetiQ and COSMIC datasets, accentuating the impact of larger disparities in time and location on observed variations in atmospheric variables.

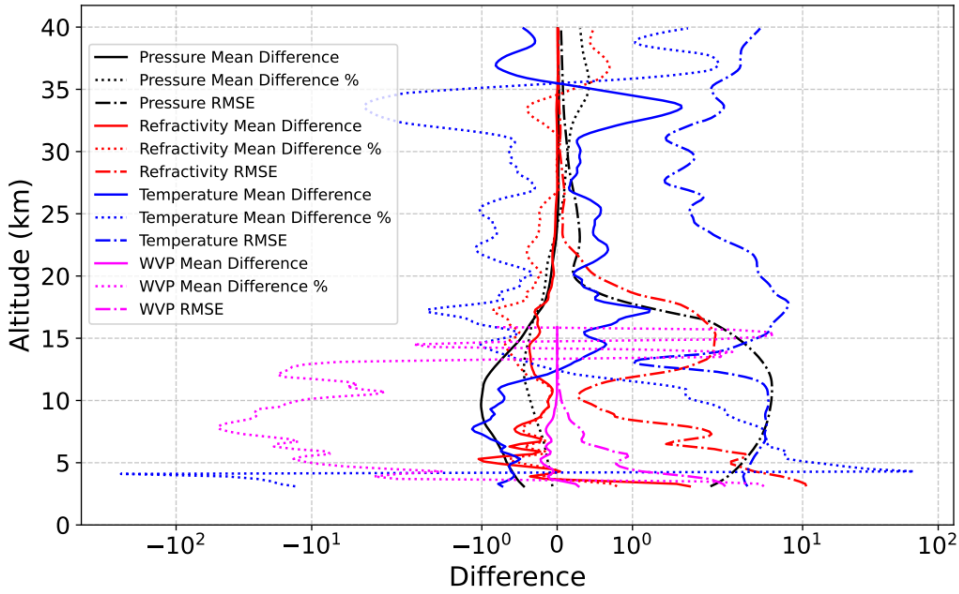

Figure 16. Mean diff., mean diff.% and RMSE between PlanetiQ and COSMIC profiles for G3 for all variables.

Table 1 summarizes the assessment of differences between variances and observations within the context of G1 observations, considering a temporal difference less than 15 minutes and a spatial deviation of 0.25° in latitude and longitude. The f-test is employed to evaluate the significance of variance differences, with a p-value greater than 0.05 indicating no substantial variance distinction between profiles. On the other hand, the t-test assesses the significance of divergence in observation profiles, with a t-stat value below the critical threshold signifying no noteworthy variation.

The f-test results for the four profile variables across the nine checkpoints reveal a lack of significant disparity in variances among the compared profiles. Furthermore, the t-stat values from the t-test analysis are consistently below the critical threshold for all observation variables. This substantiates the conclusion that there is no significant dissimilarity between the PlanetiQ and COSMIC profiles across all the examined checkpoints.

Table 1. F-test and t-test key numbers for G1 PlanetiQ-COSMIC profiles comparison.

PlanetiQ observations (filestamp)	COSMIC observations (filestamp)	f-test P value (Pres., Temp., WVP, Ref.)	T-stat (Pres., Temp., WVP, Ref.)	T-cr.
GN04.2023.353.18.15.R24	C2E2.2023.353.18.18.G31	0.99, 0.8, 0.45, 0.88	0.008, 0.24, -0.75, -0.15	1.96
GN02.2023.347.21.41.C20	C2E1.2023.347.21.39.G31	0.99, 0.87, 0.91, 0.97	0.003, 0.16, -0.11, -0.03	

 doi:10.20944/preprints202404.1137.v1

GN04.2023.348.08.07.C24	**C2E6.2023.348.08.10.G05**	0.98, 0.8, 0.29, 0.92	0.016, 0.25, 1.07, 0.1
GN04.2023.340.11.18.G23	**C2E5.2023.340.11.13.R17**	0.75, 0.73, 0.52, 0.71	-0.31, -0.33, -0.63, -0.37
GN04.2023.353.10.22.G07	**C2E2.2023.353.10.22.G07**	0.99, 0.99, 0.87, 0.99	-0.01, -0.02, -0.16, -0.02
GN02.2023.340.06.33.C41	**C2E3.2023.340.06.28.G24**	0.99, 0.94, 0.73, 0.94	0.00, 0.08, 0.35, 0.08
GN04.2023.348.08.07.E31	**C2E6.2023.348.08.10.G05**	0.98, 0.84, 0.53, 0.96	0.02, 0.2, 0.62, 0.06
GN04.2023.340.11.18.R17	**C2E5.2023.340.11.13.R17**	0.99, 0.89, 0.93, 0.98	0.00, -0.13, -0.08, 0.02
GN02.2023.342.14.23.G18	**C2E6.2023.342.14.32.R16**	0.99, 0.98, 0.75, 0.93	0.00, 0.03, 0.31, 0.08

4.3. PlanetiQ-NWP Models Comparison

4.3.1. PlanetiQ-GFS Model Comparison

Figure 17 presents a comparison of the pressure, temperature, WVP, and refractivity profiles from the PlanetiQ and GFS models for the day of year (DOY) 2023.342, characterized by an average number of occultation events. The results exhibit noteworthy differences between the two models, as highlighted by key numerical metrics.

For WVP, the overall RMSE for the wet_avn scenario is 0.23, indicating a moderate level of deviation between models. Similarly, pressure and temperature differences display an overall RMSE of 0.58 mb and 1.54°C, respectively. The refractivity differences show the most significant deviation, with a total RMSE of 1.27.

The MAD further emphasizes the disparities, showcasing values of 0.08 mb, 0.35 mb, 0.5, and 1.07°C for WVP, pressure, refractivity, and temperature, respectively. These values demonstrate the magnitude of the differences between the mission profiles and the GFS model, with temperature being the highest absolute difference

Examining the altitude-specific analysis for the altitude range (5, 20) km, the mean differences highlight nuanced variations. Notably, WVP, pressure, and temperature exhibit small mean differences of -0.002 mb, 0.15 mb, and -0.02°C, respectively. However, refractivity displays a mean difference of 0.04, emphasizing a significant shift in this parameter. WVP, pressure, refractivity, and temperature all have altitude-specific RMSE values of 0.07 mb, 0.3 mb, 0.51, and 0.85°C, respectively, indicating model precision.

 doi:10.20944/preprints202404.1137.v1

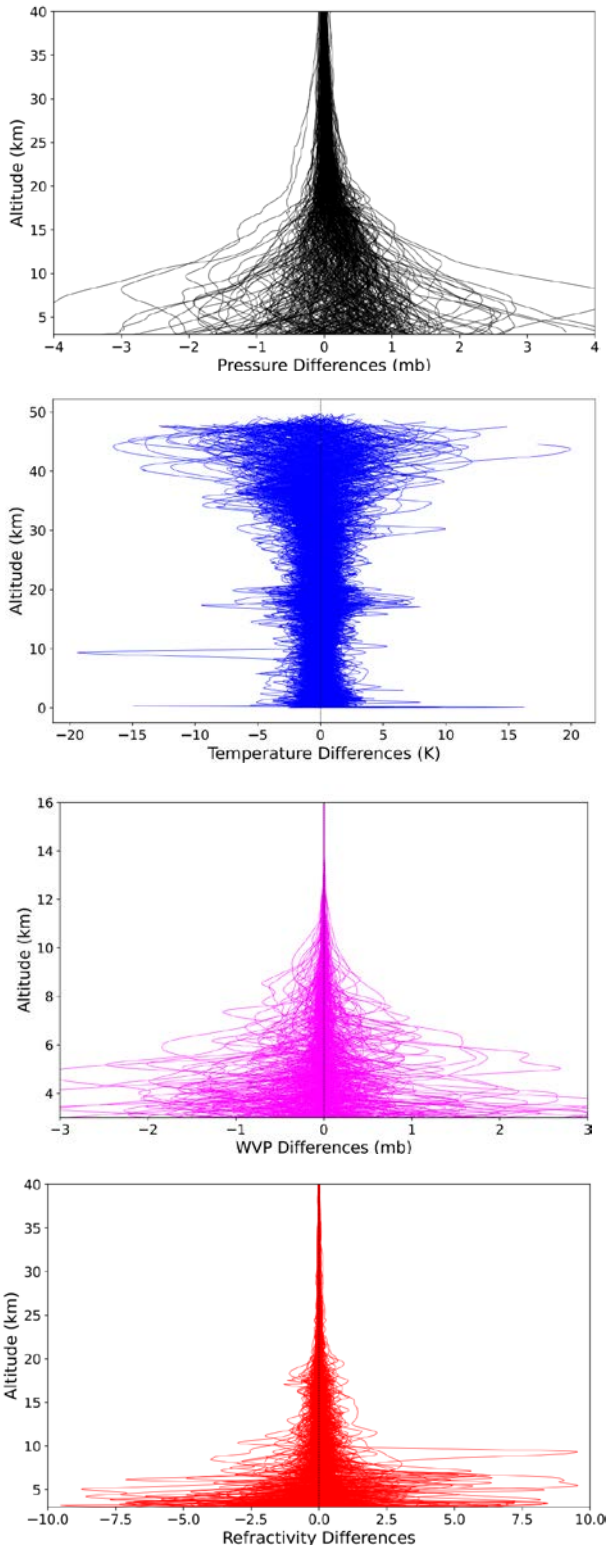

Figure 17. DOY 342 profiles differences between PlanetiQ and GFS model for all variables.

Figure 18 provides a complete comparison of various key metrics for pressure, refractivity, temperature, and WVP profiles between the PlanetIQ and ECMWF models throughout the study period. The Maximum Difference in pressure profiles is noted at 4.2 mb, with a corresponding maximum difference percentage of 0.6%. The mean difference for pressure is -0.19 mb, and the maximum RMSE is observed at 29.7 mb, occurring at an altitude of 3.0. The altitude of maximum mean difference for pressure is 14.2, and the mean difference percentage at maximum RMSE is -0.6%.

 doi:10.20944/preprints202404.1137.v1

For refractivity, the maximum difference is 1.8, and the maximum difference percentage is 0.8%. The mean difference in refractivity is -0.07, while the maximum RMSE reaches 10.4, situated at an altitude of 3.0. The altitude of maximum mean difference for refractivity is 16.3, and the mean difference percentage at the maximum RMSE is -0.8%.

Temperature profiles reveal a maximum difference of 0.46°C, with a corresponding maximum difference percentage of 3.4%. The mean difference for temperature is -0.14°C, and the maximum RMSE is 3°C, occurring at an altitude of 40.0. The altitude of maximum mean difference in temperature is 19.9°C, and the mean difference percentage at maximum RMSE is 0.6%.

WVP profiles exhibit a Maximum Diff. of 0.1, along with a Maximum Diff.% of 26.8%. The Mean Diff. for WVP is -0.02 mb, and the Maximum RMSE is 1 mb, situated at an altitude of 3.0. The Altitude of Maximum Mean Diff. for WVP is 12.9, and Mean Diff.% at Maximum RMSE is -3.3%.

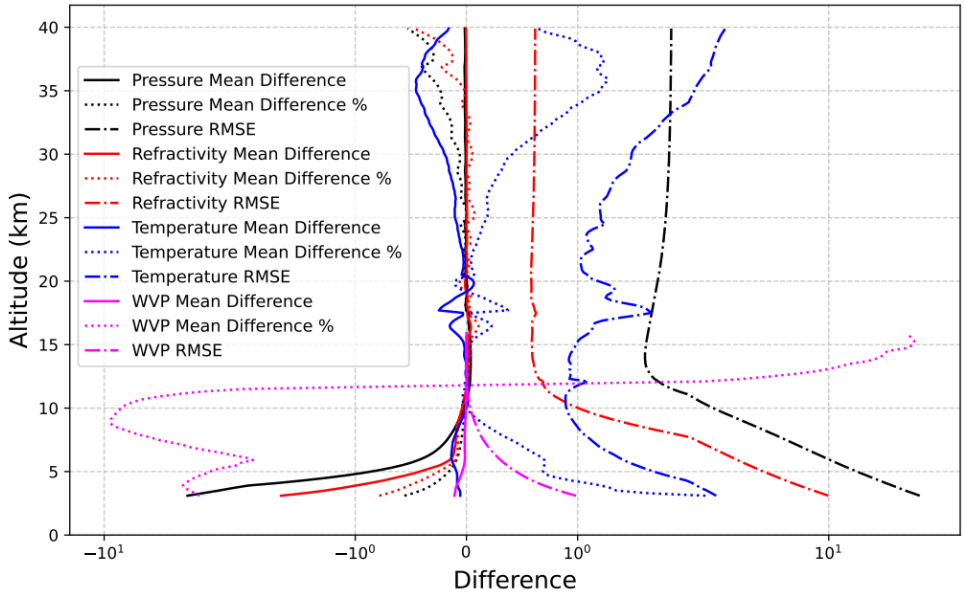

Figure 18. Mean diff., mean diff.% and RMSE between PlanetiQ and GFS model profiles for all variables. .

In Figure 19, the distribution of diff.% between PlanetIQ and GFS profiles at 3 km altitude for various variables is depicted over the study period. Pressure differences remain generally within ±0.5%, except for certain land areas in the southern hemisphere where deviations are observed. Across the globe, diff.% at 3 km altitude for pressure does not exceed ±2%.

Temperature differences, given the relatively small values of measurements at 3 km altitude, may exhibit slightly higher diff.%, but still generally remain below ±2.5%. Notably, temperature diff.% increases around the equator and pole regions, with differences elsewhere not surpassing 0.4%.

WVP difference percentage typically is less than ±0.5%, except for specific distributed regions where it may reach up to ±3%, particularly near the equator. Refractivity difference percentage generally does not exceed ±4%, concentrated around the equator, and tends to decrease moving towards the poles.

In summary, the analysis reveals that the differences in the aforementioned variables between PlanetIQ and GFS profiles at 3 km altitude are generally within acceptable limits, with occasional exceptions in specific places. The findings provide valuable insights into the performance and agreement of the two datasets, highlighting areas of interest such as the equator and pole regions where variations are more pronounced.

 doi:10.20944/preprints202404.1137.v1

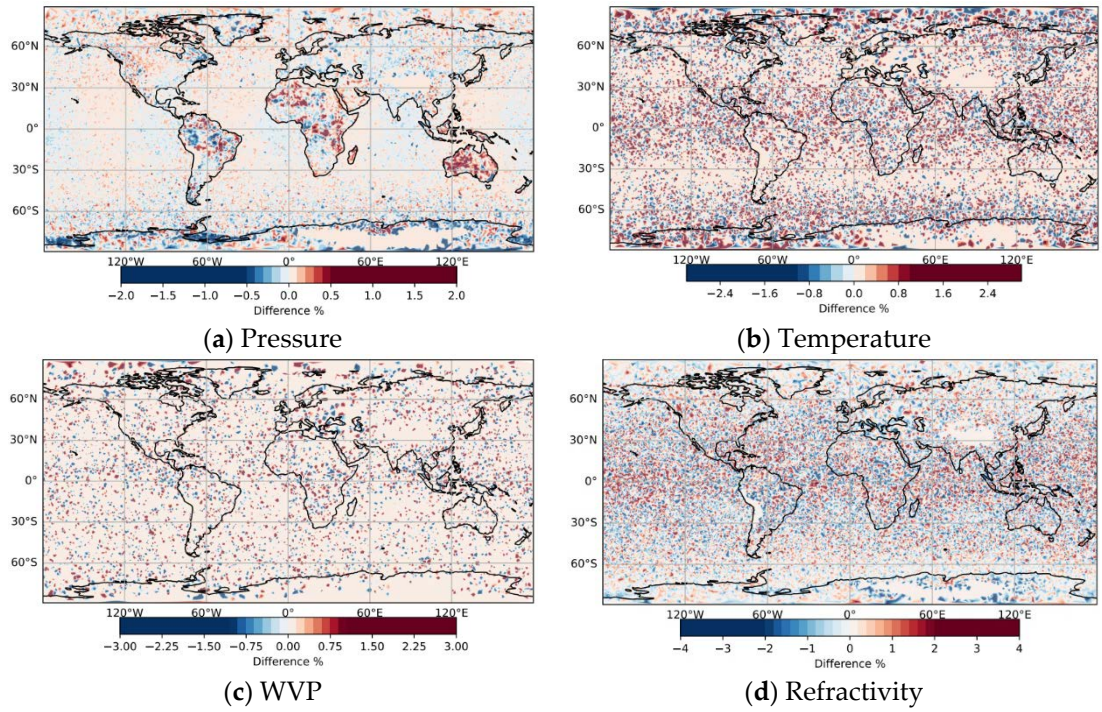

(**a**) Pressure (**b**) Temperature

(**c**) WVP (**d**) Refractivity

Figure 19. Diff.% contour maps for all variables at altitude 3 km between PlanetiQ and GFS.

4.3.3. PlanetiQ-ECMWF Model Comparison

Figure 20 presents a detailed examination of the profiles for pressure, temperature, WVP, and refractivity, comparing the PlanetIQ and GFS model on DOY 2023.342, characterized by an average number of occultation events. The results showcase substantial differences between the two models, with key numerical metrics offering insight into the extent of these variations.

For WVP, the overall RMSE for the wet_ech scenario is 0.18, signifying a relatively modest level of deviation between the mission profiles and the GFS model. Likewise, pressure and temperature differences exhibit overall RMSE values of 0.38 mb and 1.3°C, respectively. Refractivity differences demonstrate the most pronounced divergence, with an overall RMSE of 0.9 mb.

The MAD highlights the absolute magnitude of the disparities, presenting values of 0.05 mb, 0.24 mb, 0.35, and 0.9°C for WVP, pressure, refractivity, and temperature, respectively. Temperature differences are particularly noteworthy, indicating a substantial absolute difference between the two models.

Altitude-specific analysis for the range (5, 20) km reveals subtle mean differences. WVP, pressure, and temperature exhibit minor mean differences of -0.001 mb, -0.01 mb, and -0.05°C, respectively. Refractivity, however, displays a slightly larger mean difference of 0.0134, emphasizing a discernible shift in this parameter. WVP, pressure, refractivity, and temperature have altitude-specific RMSE values of 0.05 mb, 0.3 mb, 0.4, and 0.64°C, respectively, indicating model precision.

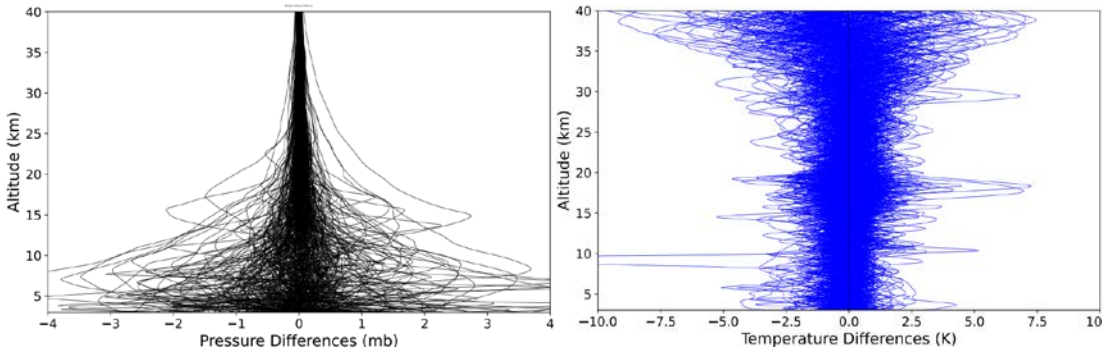

 doi:10.20944/preprints202404.1137.v1

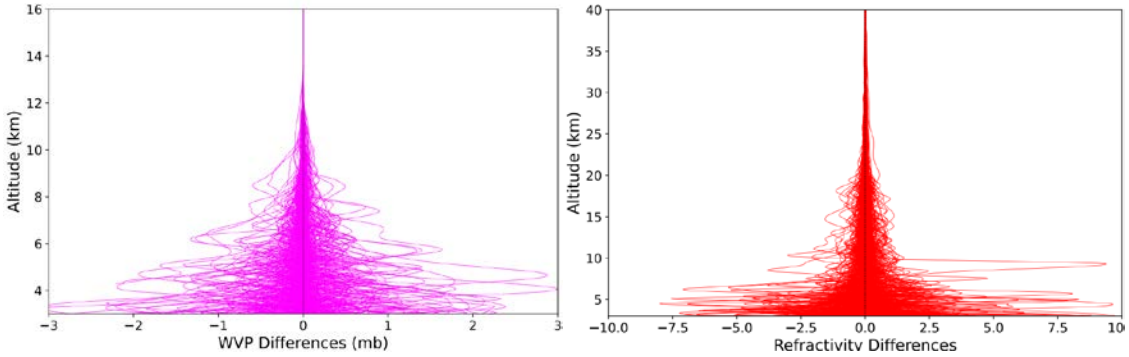

Figure 20. DOY 342 profiles differences between PlanetiQ and ECMWF model for all variables. .

Figure 21 illustrates a comprehensive comparison of the critical variables: pressure, refractivity, temperature, and WVP, between the PlanetIQ and ECMWF model profiles for the entire study period. The results provide a full overview of the differences, expressed in mean difference, maximum difference, maximum difference percentage, and RMSE metrics.

For Pressure, the maximum difference is 3.0875, with a corresponding maximum difference percentage of 0.4%. The mean difference is -0.16, with a maximum RMSE reaches 25.6. The altitude of the maximum mean difference is 25.2 km, while the maximum RMSE occurs at an altitude of 3.0 km, constituting a mean difference percentage at maximum RMSE of -0.4%.

In terms of refractivity, the maximum difference is 1.0, accompanied by a maximum difference percentage of 0.5%. The mean difference is -0.04, with the maximum RMSE of 8.8284. The altitude of the largest mean difference is 12.5 km, while the maximum RMSE occurs at 3.0 km, with a mean difference percentage of -0.5% at the maximum RMSE.

Temperature differences exhibit a maximum difference of 0.2°C and a maximum difference percentage of 10.9%. The mean difference is -0.01, with a maximum RMSE of 2.7°C. The altitude of the maximum mean difference is 32.8 km, whereas the maximum RMSE occurs at 3.0 km, with a mean difference percentage of 10.9% at the maximum RMSE.

For WVP, the maximum difference is 0.04 mb, with a maximum difference percentage of 2.7%. The mean difference is -0.004 mb, with a maximum RMSE of 0.8 mb. The altitude of the maximum mean difference is 8.0 km, while the maximum RMSE occurs at 3.0 km, with a mean difference percentage at maximum RMSE of -1.2%.

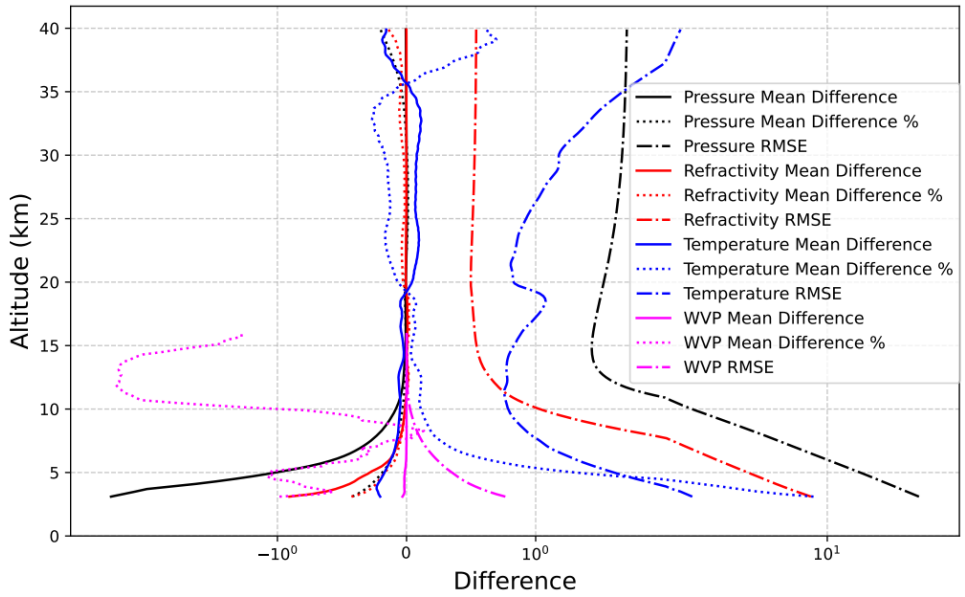

Figure 21. Mean diff., mean diff.% and RMSE between PlanetiQ and ECMWF model profiles for all variables.

 doi:10.20944/preprints202404.1137.v1

Figure 22 illustrates the percentage difference between PlanetIQ and ECMWF profiles at 3 km altitude across various variables throughout the study duration. The pressure difference remains within ±0.2%, with minor deviations in limited areas globally. Notably, there is a marginal increase in the southern pole, indicating a more favorable agreement with the ECMWF model in terms of pressure differences compared to the GFS model.

Regarding temperature difference percentage, the ECMWF exhibits a slight escalation around the equator and poles. The maximum difference reaches ±2.5% in specific regions highlighted on the map, which is slightly higher value than the GFS temperature difference.

The WVP difference is normally less than ±0.5%, except for specific distributed areas where it may reach up to ±3%, particularly around the equator. This pattern is consistent with the GFS results.

The refractivity difference typically ranges between ±4%, with higher concentrations near the equator and decreasing toward the poles. This aligns with the distribution observed in the GFS results.

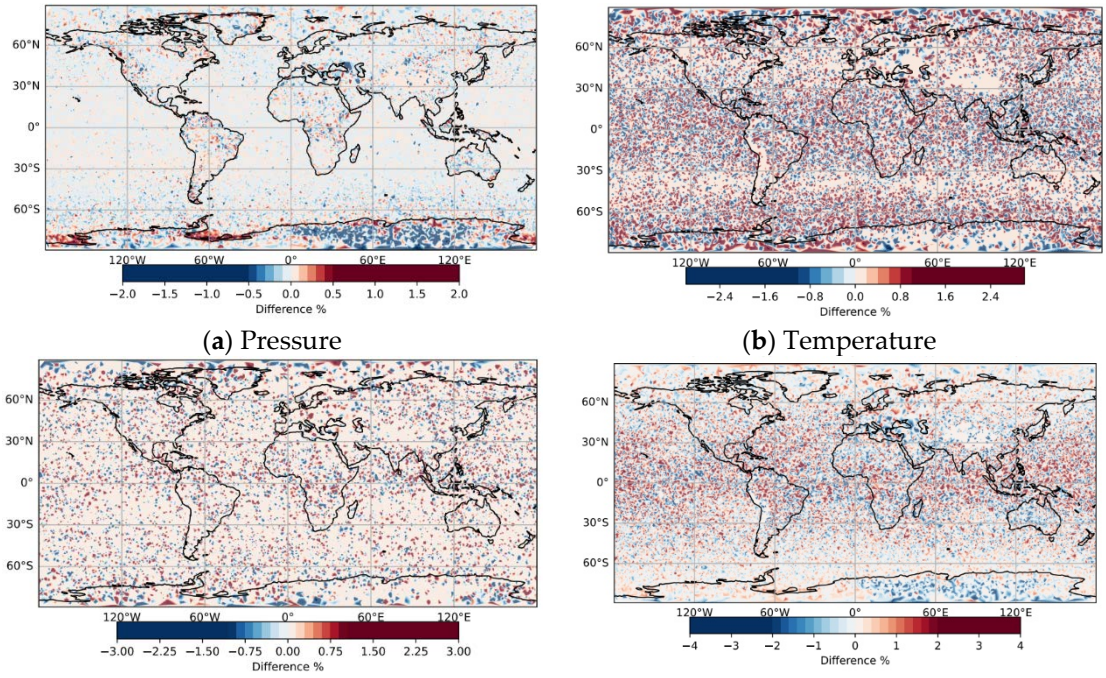

(**a**) Pressure (**b**) Temperature

(**c**) WVP (**d**) Refractivity

Figure 22. Diff.% contour maps for all variables at altitude 3 km between PlanetiQ and ECMWF.

Figure 23 shows the boxplot for the RMSE across atmospheric variables to show the differences between the PlanetiQ profiles and GFS and ECMWF profiles. The RMSE values for differences between PlanetIQ observations and ECMWF/GFS models across meteorological parameters reveal notable distinctions. The median air pressure estimates for the ECMWF and GFS are around 1.67 mb and 1.82 mb, respectively. GFS has a slightly higher mean RMSE of 3.47 mb compared to ECMWF's 3.28 mb, indicating a larger overall discrepancy. The ECMWF has a moderate IQR of 0.14, while the GFS has a little lower IQR of 0.10 mb, with similar whisker min and max values.

The ECMWF and GFS have different median values for refractivity, with 0.53 and 0.61 respectively. The GFS has a slightly higher mean RMSE, 1.20, than the ECMWF's 1.11. The IQR for refractivity in GFS is notably smaller at 0.05, reflecting a more concentrated spread, whereas the ECMWF's IQR is 0.14. Whisker min and max values for both models fall within their respective IQRs.

For temperature, the ECMWF and GFS have median values of 1.05 and 1.29, respectively, with mean RMSE values of 1.21°C and 1.49°C. The ECMWF temperature data has a larger IQR of 0.60 compared to the GFS's 0.69°C. Whisker min and max values for both models extend beyond their respective IQRs, indicating the presence of outliers.

In case of WVP, the ECMWF and GFS have median values of 0.19 mb and 0.05 mb, respectively. The GFS has a lower mean RMSE (0.18 mb) than the ECMWF (0.25 mb). The IQR for WVP in ECMWF

 doi:10.20944/preprints202404.1137.v1

is 0.30 mb, reflecting a broader spread, while the GFS IQR is 0.26 mb. Whisker min and max values in WVP exhibit differences in distribution for both models.

In summary, the varying levels of agreement between PlanetIQ observations and ECMWF/GFS models across meteorological parameters are evident from the differences in mean RMSE, IQR, and whisker values.

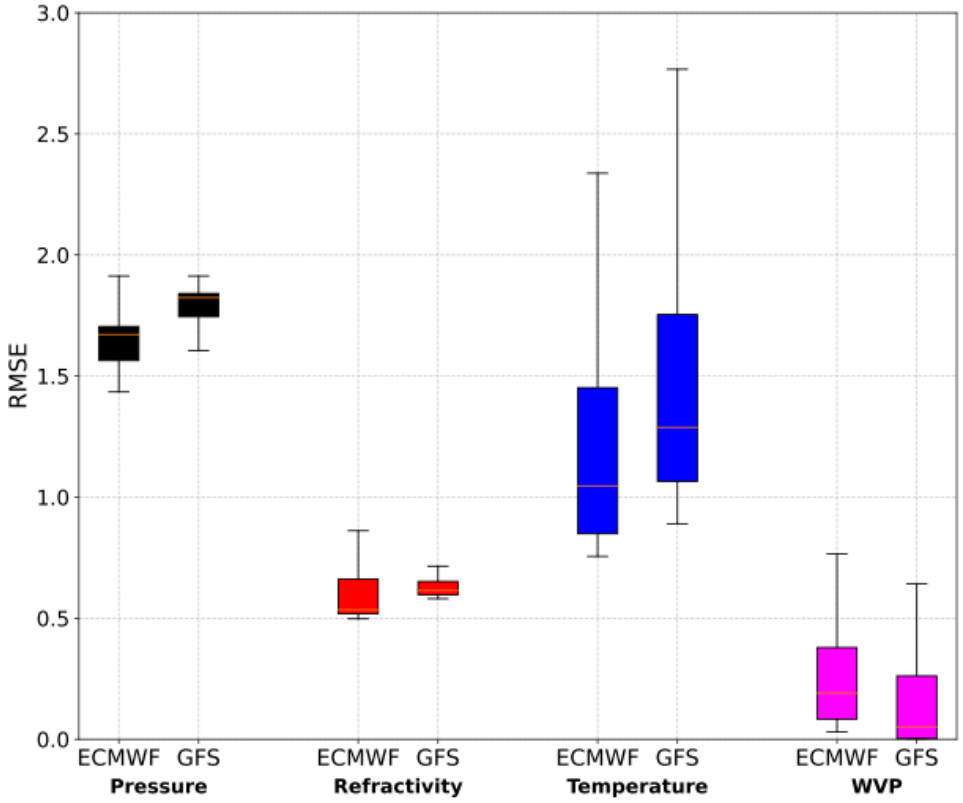

Figure 23. Boxplot for RMSE values between PlanetiQ and each of GFS and ECMWF models for each variable.

To investigate the variance disparities between PlanetiQ profiles and GFS and ECMWF models, as well as the differences in observational profiles, an f-test and t-test were employed, respectively. Table 2 presents the findings from these tests conducted on random samples of mission profiles, with six checkpoints spaced 25 to 50 days apart.

The f-test results show no significant differences in variance across all profile comparisons between PlanetiQ profiles and GFS and ECMWF models, with the exception of the GN02.2023.100.00.10.R20 WVP profile. This specific profile exhibits a noteworthy difference in variances between the profiles of the PlanetiQ and the two models.

Furthermore, the t-test findings for the six checkpoints indicate a lack of significant differences between PlanetiQ profile observations and model profiles, except for the WVP profile at the same checkpoint when compared to both models. It is crucial to note that the observed significant difference in WVP is not considered a limitation in the production of PlanetiQ WVP data. This discrepancy is attributed to small temporal and spatial variations. Given that NWP models generate spatial and temporal profiles from disparate observations, which are not necessarily in the same location and time, spatial and temporal interpolation in NWP models may introduce unreliability into the WVP profiles they produce.

Table 2. F-test and t-test key numbers for samples of PlanetiQ profiles comparison with GFS and ECMWF models.

PlanetiQ observations (filestamp)	Model	f-test P value	T-stat	T-cr.

 doi:10.20944/preprints202404.1137.v1

		(Pres., Temp., WVP, Ref.)	(Pres., Temp., WVP, Ref.)	
GN02.2023.100.00.10.R20	GFS ECMWF	0.98, 0.4, 0.00, 0.98 0.96, 0.17, 0.00, 0.94	-0.015, 0.82, 8.4, -0.02 -0.05, 0.01, 8.4, -0.08	
GN02.2023.125.00.44.E11	GFS ECMWF	0.98, 0.87, 0.6, 0.99 0.99, 0.95, 0.66, 0.99	0.03, -0.16, -0.51, 0.01 0.02, -0.07, -0.45, -0.01	
GN03.2023.200.12.47.G27	GFS ECMWF	0.9, 0.98, 0.33, 0.89 0.95, 0.99, 0.87, 0.93	-0.12, 0.02, 0.98, -0.135 0.05, -0.02, 0.17, 0.08	1.96
GN02.2023.250.00.04.G12	GFS ECMWF	1, 0.92, 0.18, 0.99 0.99, 1, 0.52, 0.99	0.00, -0.1, -1.33, 0.01 -0.01, 0.00, 0.64, 0.01	
GN02.2023.300.00.25.E09	GFS ECMWF	0.93, 0.58, 0.09, 0.88 0.93, 0.69, 0.62, 0.92	0.09, -0.54, 1.7, 0.02 0.08, -0.39, 0.49, 0.1	
GN02.2023.350.01.00.C44	GFS ECMWF	0.99, 0.92, 0.87, 0.95 0.97, 0.93, 0.87, 0.93	0.01, 0.01, 0.15, 0.05 0.02, -0.02, 0.17, 0.06	

5. Conclusions

PlanetiQ's RO mission, as illustrated through the GNOMES satellites, strives to establish the world's most advanced atmospheric observing system. This is achieved by deploying cutting-edge RO sensors to ensure precise and frequent measurements, ultimately enhancing global weather forecasting capabilities. The present research's objective is to investigate the temporal and spatial distribution of observations and evaluate them by comparing them to atmospheric data from the COSMIC and NWP models.

The mission aims to deploy 20 RO satellites, each generating 2500 ROE per day, for a total of 50,000 ROE per day across the constellation. Data from the GN02, GN03, and GN04 satellites reveal average observation numbers of 1099, 1313, and 1843 ROE/day, respectively. The daily occurrence of observations by the satellite constellation exhibits a generally well-distributed pattern, with minor shortages reported in the equatorial and Polar Regions.

The pressure, temperature, WVP, and refractivity profiles of PlanetiQ were compared to those of COSMIC profiles. A detailed assessment of differences was carried out using statistical analyses, including the f-test and t-test. Single-profile comparisons at specific checkpoints reveal reasonable differences within acceptable ranges. Multi-profile comparisons across various checkpoints further corroborate the insignificance of differences between variables and observation variances.

Additionally, differences between observation variables and GFS/ECMWF NWP models were evaluated to ensure compatibility. The statistical tests demonstrate no significant differences between PlanetiQ profiles and NWP model variances and observations, with the exception of a single point in the WVP profiles. This discrepancy is attributed to interpolation methods used in deducing WVP values in the NWP models.

In conclusion, while the number of RO observations per satellite is substantial, it has not yet reached the desired quantity. The spatial and temporal distribution of observations is generally satisfactory, with minor deficiencies at equatorial and polar areas. Insignificant differences from COSMIC profiles affirm the high-definition quality of the collected data. Except for a justifiable variation in WVP, the differences with NWP models are mostly insignificant.

Author Contributions: Conceptualization, I.F.A.; Methodology, I.F.A., M.A. and M.S.Y.; Software, I.F.A. and M.S.Y.; Validation, I.F.A. and M.S.Y.; Formal Analysis, I.F.A., M.A. and M.S.Y.; Investigation, I.F.A. and M.A.; Resources, M.A.; Data Curation, I.F.A. and M.S.Y.; Writing – Original Draft Preparation, I.F.A.; Writing – Review & Editing, M.S.Y. and M.A.; Visualization, M.S.Y. and M.A.; Supervision, M.S.Y.; Project Administration, M.A.; Funding Acquisition, M.A. All authors have read and agreed to the published version of the manuscript.

Funding: This research study is funded by the Researchers Supporting Project number (RSPD2024R902), King Saud University, Riyadh, Saudi Arabia.

Data Availability Statement: The raw data supporting the conclusions of this article will be made available by the authors on request.

Informed Consent Statement: Not applicable.

Acknowledgment: The authors extend their appreciation to the Researchers Supporting Project number (RSPD2024R902), King Saud University, Riyadh, Saudi Arabia, for funding this work.

Conflict of Interests: The authors declare that they have no known competing financial interests or personal relationships that could have appeared to influence the work reported in this paper.

Ethical approval: This article does not contain any studies with human participants or animals performed by any of the authors.

Informed consent: Not applicable.

References

1. Ghoniem, I. F., Mousa, A. E.-K., & El-Fiky, G. (2020). Optimization of GNSS-RO LEO satellite orbits for Egypt and the Middle East region. Alexandria Engineering Journal, 59(1), 389-397. https://doi.org/10.1016/j.aej.2020.01.006
2. PlanetiQ. (2024, February 1). Technology. PlanetiQ. https://planetiq.com/technology/
3. Bai, W., Deng, N., Sun, Y., Du, Q., Xia, J., Wang, X., ... & Tan, G. (2020). Applications of GNSS-RO to Numerical Weather Prediction and Tropical Cyclone Forecast. Atmosphere, 11(11), 1204. https://doi.org/10.3390/atmos11111204
4. Kursinski, E. R., Hajj, G. A., Schofield, J. T., Linfield, R. P., & Hardy, K. R. (1997). Observing Earth's atmosphere with radio occultation measurements using the Global Positioning System. Journal of Geophysical Research: Atmospheres, 102(D19), 23429-23465.
5. Qiu, C., Wang, X., Zhou, K., Zhang, J., Chen, Y., Li, H., ... & Yuan, H. (2023). Comparative Assessment of Spire and COSMIC-2 Radio Occultation Data Quality. Remote Sens., 15, 5082. https://doi.org/10.3390/rs15215082
6. Zhang, H., Huangfu, J., Wang, X., Chen, W., Peng, W., Tang, Q., ... & Xue, Z. (2022). Comparative Analysis of Binhu and Cosmic-2 Radio Occultation Data. Remote Sens., 14, 4958. https://doi.org/10.3390/rs14194958
7. Ahmed, I. F., Abd El-Fatah, M. A., Mousa, A. E.-K., & El-Fiky, G. (2022). Analysis of the differences between GPS radio occultation and radiosonde atmosphere profiles in Egypt. The Egyptian Journal of Remote Sensing and Space Science, 25(2), 491-500. https://doi.org/10.1016/j.ejrs.2022.02.006
8. Melbourne, W. G., Davis, E., Duncan, C., Hajj, G., Hardy, K., Kursinski, E., ... & Yunck, T. P. (1994). The application of spaceborne GPS to atmospheric limb sounding and global change monitoring. JPL Publ. 94–18, Pasadena, CA.
9. Rocken, C., Anthes, R., Exner, M., Hunt, D., Sokolovskiy, S., Ware, R., ... & Zou, X. (1997). Analysis and validation of GPS/MET data in the neutral atmosphere. J. Geophys. Res., 102, 29849–29866. [doi: 10.1029/97JD02400](doi: 10.1029/97JD02400)
10. Mousa, A., Aoyama, Y., & Tsuda, T. (2006). A simulation analysis to optimize orbits for a tropical GPS radio occultation mission. Earth Planets Space, 58, 919–925.
11. Pavelyev, A., Pavelyev, A., Matyugov, S., Yakovlev, O., Liou, Y.-A., Zhang, K., & Wickert, J. (2013). Radio Wave Propagation Phenomena from GPS Occultation Data Analysis. InTech. [doi: 10.5772/55480](doi: 10.5772/55480)
12. Li, M., Yue, X., Wan, W., & Schreiner, W. (2020). Characterizing Ionospheric Effect on GNSS Radio Occultation Atmospheric Bending Angle. Journal of Geophysical Research: Space Physics. https://doi.org/10.1029/2019JA027471
13. Liu, H., Zou, X., Shao, H., Anthes, R., Chang, J., Tseng, J-H., & Wang, B. (2001). Impact of GPS/MET bending angle profiles on assimilation and forecasts for the period June 20-30. J. Geophys. Res., 106, 31771–31786.
14. Fjeldbo, G., Kliore, J., & Eshleman, V. (1971). The neutral atmosphere of Venus as studied with the Mariner V radio occultation experiments. The Astronomical Journal, 76, 123-140.
15. Prol, F. S., Hoque, M. M., Hernández-Pajares, M., Yuan, L., Olivares-Pulido, G., von Engeln, A., ... (2023). Study of Ionospheric Bending Angle and Scintillation Profiles Derived by GNSS Radio-Occultation with MetOp-A Satellite. Remote Sens., 15, 1663. https://doi.org/10.3390/rs15061663
16. Shen, Z., He, Q., Li, L., Zhang, K., & Wu, S. (2020). Daily Climatological Fields Based on GNSS Radio Occultation Measurements: A Feasibility Study. In: Sun, J., Yang, C., & Xie, J. (Eds.), China Satellite Navigation Conference (CSNC) 2020 Proceedings: Volume I. Springer. https://doi.org/10.1007/978-981-15-3707-3_39
17. Camacho-Lara, S. (2016). Current and Future GNSS and Their Augmentation Systems. In: Pelton, J., Madry, S., & Camacho-Lara, S. (Eds.), Handbook of Satellite Applications. Springer. https://doi.org/10.1007/978-1-4614-6423-5_25-3

 doi:10.20944/preprints202404.1137.v1

18. Innerkofler, J., Kirchengast, G., Schwärz, M., Marquardt, C., & Andres, Y. (2023). GNSS radio occultation excess-phase processing for climate applications including uncertainty estimation. Atmospheric Measurement Techniques, 16, 5217-5247. https://doi.org/10.5194/amt-16-5217-2023
19. Pirscher, B. (2010). Multi-satellite climatologies of fundamental atmospheric variables from radio occultation and their validation (Ph.D. thesis), Wegener Center Verlag Graz, Austria, Sci. Rep. 33-2010.
20. Alizadeh, M., Wijaya, D., Hobiger, T., Weber, R., & Schuh, H. (2013). Atmospheric Effects in Space Geodesy. https://doi.org/10.1007/978-3-642-36932-2_2
21. Born, M., & Wolf, E. (1964). Principles of Optics. New York, NY: Pergamon.
22. Xie, F., Syndergaard, S., Kursinski, E. R., & Herman, B. M. (2006). An approach for retrieving marine boundary layer refractivity from GPS occultation data in the presence of superrefraction. J. Atmos. Ocean. Technol., 23(11), 1629–1644.
23. University Corporation for Atmospheric Research. (2024, February 1). UCAR. https://ucar.edu/
24. European Centre for Medium-Range Weather Forecasts. (2023, December 12). ECMWF, https://www.ecmwf.int/
25. National Oceanic and Atmospheric Administration. (2023, December 30). NOAA, https://www.noaa.gov/